Applied Energy 322 (2022) 119535

Contents lists available at ScienceDirect

Applied Energy

journal homepage: www.elsevier.com/locate/apenergy

Exploring the techno-economic feasibility of new bioeconomy concepts: Solar-assisted thermochemical biorefineries

R.E. Gutiérrez [a,b], K. Guerra [a], P. Haro [a,*]

[a] Chemical and Environmental Engineering Department. Escuela Técnica Superior de Ingeniería, Universidad de Sevilla, Camino de los Descubrimientos s/n., 41092 Seville, Spain
[b] Postgraduate Faculty, Universidad de las Américas Quito, Avenida de los Granados, E12-41 y Colimes Quito, Ecuador

HIGHLIGHTS

- Three designs for dimethyl ether (DME) production using biomass and solar energy.
- Utility supply approach is used favoring a two-way synergy between solar and biomass.
- Solar power allows positive electricity balances and a fuel upgrading of up to 4%.
- Solar-assisted scenarios show higher product conversion but lower overall efficiency.
- DME minimum selling prices are only moderately increased compared to base scenarios.

GRAPHICAL ABSTRACT

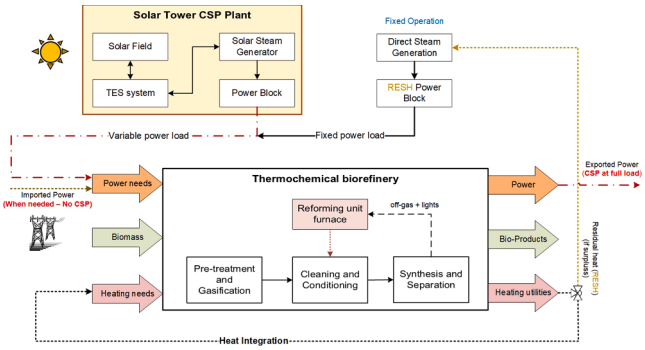

ARTICLE INFO

Keywords:
Biorefinery Processes
Solar Fuels
Dimethyl Ether
Concentrated Solar Power
Techno-economic Assessment

ABSTRACT

Integrating thermochemical biomass conversion and solar thermal energy is an emerging concept for the sustainable production of electricity, biofuels, and other renewable products. This study uses a utility supply approach to assess the techno-economic feasibility of thermochemical biorefineries (TBRF) assisted by concentrated solar power (CSP) systems. Three TBRF scenarios were modelled to produce dimethyl ether (DME) from gasified biomass (500 MW_{th}), considering different alternatives for syngas upgrading. A CSP plant of 50 MW_e and 15 h of thermal energy storage (TES) was incorporated to increase the system power generation. The assessment of the six scenarios (3 stand-alone and 3 CSP-assisted) was based on a specific location to show its potential: the solar resource of Seville (Spain) and the electricity prices in the Iberian market, both at hourly resolution. The CSP-assisted scenarios show fuel upgrading in the range of 2–4%, up to 85% of electricity demand coverage and power surpluses of up to 52% of its annual demand. However, the inclusion of a CSP block leads to an increase in investment costs of up to 74% and a decrease in the internal rate of return (IRR) of 9.2 points compared to a stand-alone TRBF. The DME minimum selling price ranged from 14 to 18.1 USD/GJ for the stand-alone scenarios and between 18.3 and 21.2 USD/GJ for the CSP-assisted scenarios. Furthermore, these results suggest that modular integration based on commercially available technologies may constitute a first step towards the feasibility of future biorefineries.

* Corresponding author.
E-mail address: pedrogh@us.es (P. Haro).

https://doi.org/10.1016/j.apenergy.2022.119535
Received 28 February 2022; Received in revised form 5 June 2022; Accepted 19 June 2022
Available online 29 June 2022

Nomenclature

DCC	direct capital costs (MUSD)
FOC	fixed operation costs (MUSD/y)
ICC	indirect capital costs (MUSD)
$\eta_{th\ total}$	energy efficiency (% HHV)
$\eta_{th\ product}$	product efficiency (% HHV)
PEC	purchase cost of equipment (MUSD)
S	stoichiometric ratio (-)
TOC	total operation costs (MUSD/y)
TPI	total plant investment (MUSD)
VOC	variable operation costs (MUSD/y)

Abbreviations

BTL	biomass-to-liquids
CEPCI	chemical engineering plant cost index
CSP	concentrated solar power
CSTE	concentrating solar thermal energy
DCFBG	dual circulant fluidized bed gasifier
DME	dimethyl ether
DMSP	DME minimum selling price
DNI	direct normal irradiation
GHI	global horizontal irradiation
GHSV	gas hourly space velocity
HEN	heat exchanger network
HHV	high heating value
HPS	high pressure steam
HRSG	heat recovery steam generation
HTF	heat transfer fluid
IRR	internal rate of return
LCOE	levelized cost of electricity
LPS	low pressure steam
MIBEL	Iberian electricity market (Spanish acronym)
MEA	monoethanolamine
MSP	minimum selling price
NPV	net present value
NREL	National Renewable Energy Laboratory
NRTL-RK	non-random two liquid with the Redlich-Kwong equation of state
PPA	power purchase agreement
PSA	pressure swing absorption
PV	photovoltaic
RESH	residual heat
RKS-BM	Redlich–Kwong–Soave with Boston–Mathias alpha function
SAM	system advisor model
SC(i)	scenarios, i ranges from 1 to 3
SR	steam reformer
ST	solar tower
TBRF	thermochemical biorefinery
TES	thermal energy storage
TMY	typical meteorological year
TR	tar cracker/reformer
TRL	technological readiness level
WGS	water gas shift reaction
WHSV	weight hourly space velocity

1. Introduction

The path towards economic decarbonization calls for the substitution of hydrocarbons used in power generation and as precursors for transport fuels, chemicals and other industrial supplies [1]. Nowadays, biomass as a carbon source is of great interest due to its contribution to reducing greenhouse gas emissions. The conversion of biomass can occur through biochemical (e.g., enzymatic hydrolysis and fermentation) or thermochemical processes (e.g., torrefaction, pyrolysis, gasification and hydrothermal treatments) in complex structures called biorefineries [2]. Thermochemical biorefinery (TBRF) is a promising option due to the possibility to take advantage of some of the know-how and technology developed by the petrochemical industry. However, TBRFs are investment-intensive facilities, require a large scale of installation to be profitable and rely on currently not fully commercial technologies [3].

One of the most attractive TBRF is based on the syngas platform, where syngas is generated through the thermal gasification of biomass and waste. A great deal of research has been conducted to assess the techno-economic feasibility of these schemes [4]. Syngas-platform biorefineries have been proposed either for a single product (i.e., biomass-to-liquids processes (BTL)) [5] or for polygeneration using other platform chemicals as intermediates [6]. A fraction of the feedstock is usually combusted to meet some or all of the energy needs of these processes [7]. Although this may favor the system energy integration, it also limits its bioproduct generation performance by using carbonaceous resources in lower value-added applications. This limitation has increased interest in integrating other renewable sources such as geothermal, solar and wind to supply the heat and electricity needs of the biorefinery [8]. Among these, solar energy is projected to be one of the most promising options due to the abundance and availability of the resource (depending on location) and the maturity of solar power generation technologies (i.e., photovoltaic (PV) and thermal). Unlike PV systems, concentrating solar thermal energy (CSTE) can provide power as well as medium and high-temperature process heat. In addition, the availability of thermal energy storage systems (TES) and the possibility of hybridization with other thermal systems make CSTE a highly suitable and dispatchable option [9]. The continuous operation of TBRFs highlights the role of CSP as a flexible utility provider.

CSTE can be integrated into TBRFs mainly following two different approaches: i) the direct supply of the heat required to drive chemical reactions in highly endothermic processes through so-called solar reactors and ii) the supply of utilities such as steam or electricity consumed in different sections of the plant. Several studies have analyzed the application of solar heat to run thermochemical reactors commonly used in TBRF concepts. For example, the solar-assisted biomass gasification in a directly irradiated packed bed reactor was addressed in [10], while an indirectly irradiated fluidized bed reactor was analyzed in [11]. Besides, the possibility of using the bed material (solid particles) as heat transfer fluid in a solar-driven dual fluidized bed reactor is assessed in [12]. Other studies have also addressed the integration of CSTE in steam reforming processes, units commonly selected for syngas upgrading in TBRFs. For example, a directly irradiated methane reforming reactor for low-carbon hydrogen production is investigated in [13] and a membrane reactor using molten salts as heat carrier is experimentally investigated at a pilot scale in [14]. Solar-assisted gasification of biomass has been thoroughly reviewed in [7], while progress on solar-assisted reforming systems is discussed in [15].

In the literature, studies of solar-assisted TBRFs are commonly based on structures in which the central unit is a solar thermochemical reactor. For instance, a solar-assisted gasification-based biorefinery for methanol and electricity generation is evaluated in [16]. Similarly, a multipurpose system for H_2, electricity and heat generation from a solar tower gasification system is assessed in [17]. These studies have considered strategies to deal with the intermittency of the solar resource, such as oversizing the solar field and storing excess syngas to be released at

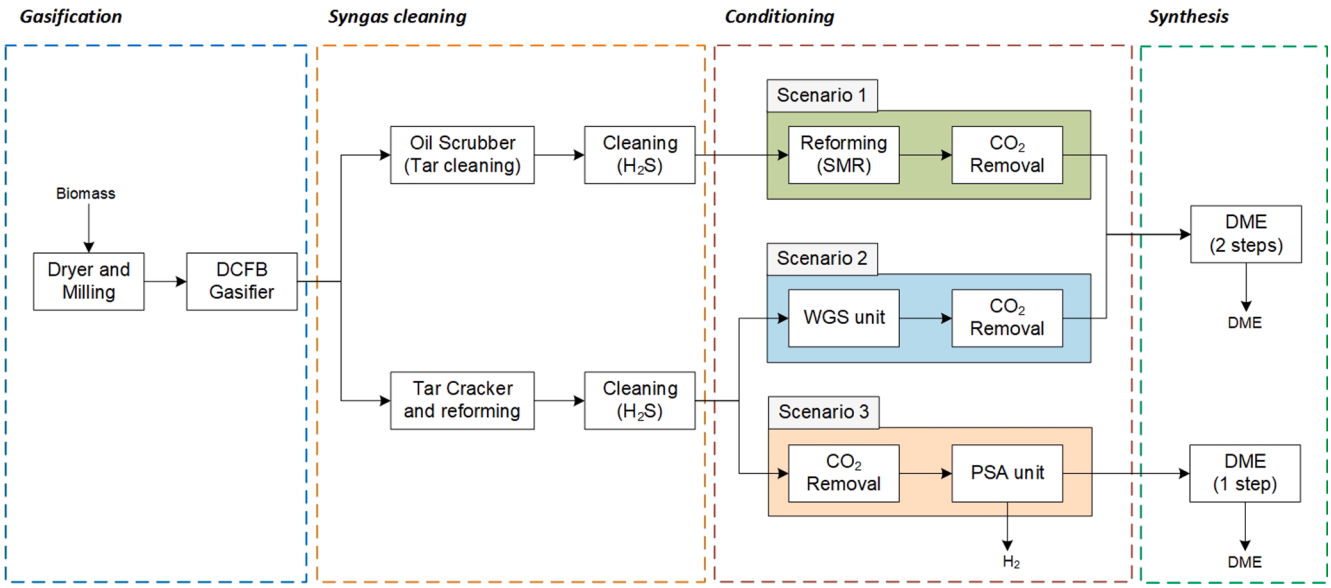

Fig. 1. Overview of selected scenarios for biomass-based DME biorefineries to be assessed in this study.

times of low or no solar irradiation. The gasification block is followed by conventional syngas cleaning and conditioning sections and a product synthesis loop in both studies. The results show the theoretical potential for solar reactor-based biorefineries to achieve higher energy efficiencies and reasonable economic competitiveness. However, further research is still needed on significant issues, such as reactor design, operation, and scalability, limiting the application and deployment of these technologies.

The previous studies focused on a reactor-level integration of solar energy to maximize the solar share in final products (i.e., fuels) and increase the energy efficiency of the entire process [12]. However, substantial technological, operational, and economic challenges still need to be overcome before solar reactors can be considered feasible solutions. The high complexity, variety of technological options, and the early stages of technological development of such systems also need to be considered [7]. Process issues such as high operating temperature and constant syngas supply (flowrate and composition) require further development of heat-transfer materials and thermal storage or hybridization options. Designing and scaling up solar reactors to economically attractive sizes for coupling to a TBRF is an issue that is yet to be solved [18]. Consequently, these issues highlight the importance of addressing further possibilities for integration that would favor the commercial development of solar-assisted biorefineries in the near future.

In contrast to the concept of solar reactor-based biorefineries, the CSTE integration approach relies on well-established technologies such as commercial concentrated solar power plants (CSP), aiming for utility supply and co-product. This approach enables decoupling between resources and represents a less technologically complex and more scalable alternative. However, only a few studies have analyzed this approach, although only for biochemical biorefineries and other renewable systems, but not in the case of a thermochemical biorefinery. For instance, the integration of PV and CSP systems in a biochemical biorefinery based on corn stover hydrolysis was analyzed in [19]. Similarly, a few conceptual alternatives for supplying electricity and heat from solar thermal and/or PV systems to an ethanol biorefinery were discussed in [8]. To the best of our knowledge, the integration of state-of-the-art CSP units into TBRFs (according to the second approach mentioned earlier) has not been addressed. This study contributes to filling this gap by assessing the techno-economic feasibility of a biomass-derived dimethyl ether (DME) biorefinery assisted by a molten salts solar tower (ST) plant. The aim is to provide insights into the performance of solar-assisted TBRFs by assessing their operation on an annualized scale with hourly resolution. This time resolution allows integrating the effect of solar intermittency and thermal storage system in the supply of utilities for both self-consumption and export.

Considering two routes for DME synthesis (i.e., 1 and 2 steps) allows addressing multiple combinations between the gasification and syngas conditioning units [6]. Therefore, DME has been chosen as the reference product to evaluate the system performance through different technological options for syngas upgrading and compare them based on the same final product (which makes the comparison fairer). DME is a product of great interest due to its potential as a transport fuel, suitable for use in conventional diesel ignition engines, as well as a commodity for the petrochemical industry [3,20]. In addition, DME can be used as a platform chemical to synthesize other products in polygeneration biorefineries. A specific location has been selected to provide an in-depth assessment with a twofold objective. Firstly, to assess the combined impact of real solar resource and the electricity market prices on the biorefinery. Secondly, to address the economic implications of assuming different trading mechanisms for buying and selling electricity as a co-product (e.g., by Power Purchase Agreements (PPAs) or by day-ahead market-imposed prices).

Modular integration based on commercially available systems seems to be the first real step towards the feasibility of solar-aided biorefineries. The support of CSP systems to the biorefinery allows extending the energy integration, prioritizing the use of the highest quality heat sources for the highest value applications. This concept could lead to a lower import of utilities and a higher yield of bioproducts without affecting the TBRF plant size to the design particularities of a solar reactor. In addition, the selected approach favors a two-way synergy between solar energy and biomass. For example, the residual heat from the TBRF can be used to increase the electrical generation of the CSP system, which at the same time is used to meet the electrical demand of the entire structure.

The paper is structured as follows: the concept used for integrating the CSP system in the biorefinery and the differences between the TBRF configurations are presented in section 2. In section 3, the techno-economic design parameters included in the modelling of all biorefinery blocks and the related simulation process are described in detail. In section 4, the main findings of the study are presented and discussed. Finally, the conclusions are included in section 5.

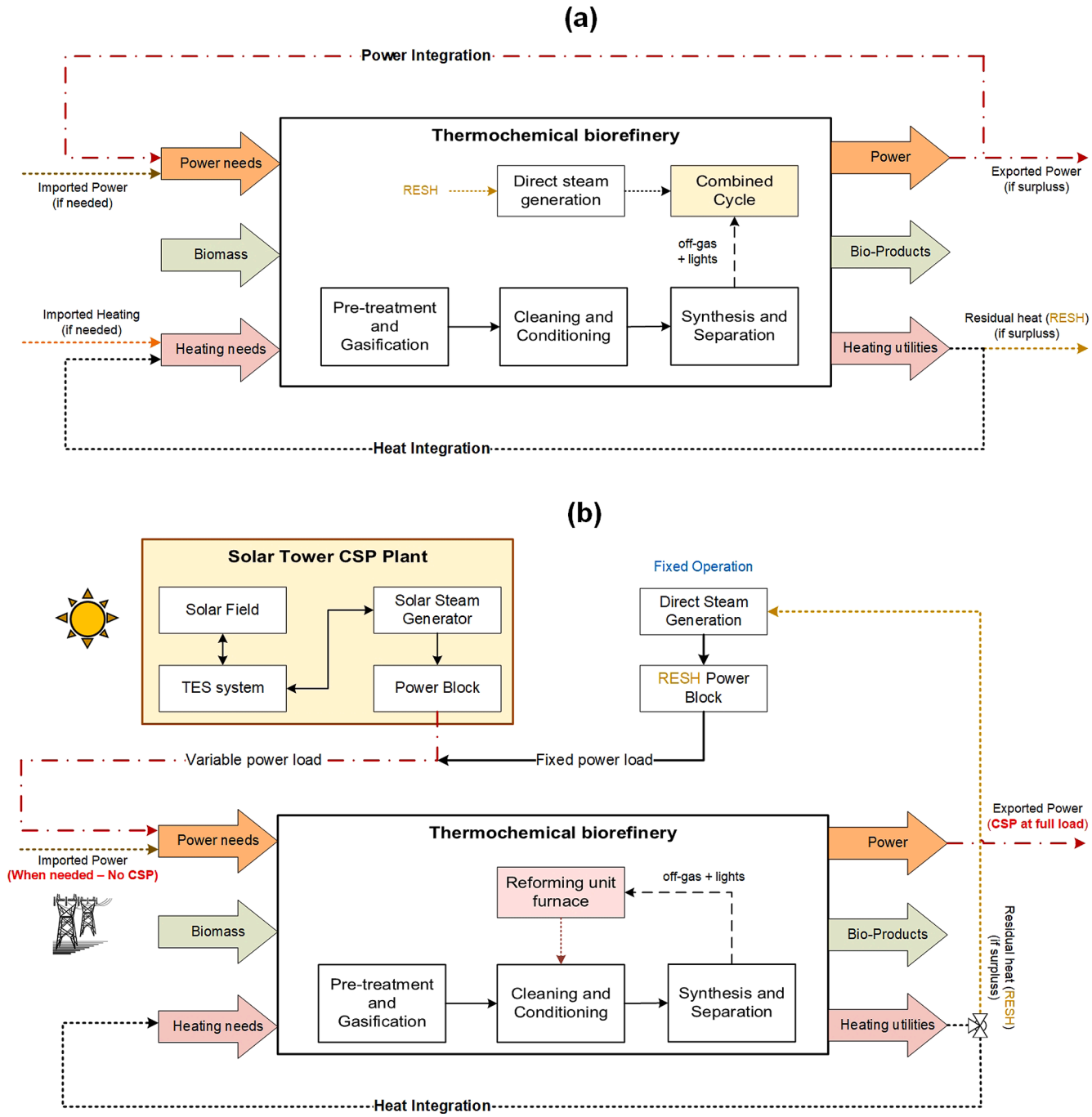

Fig. 2. Concept schemes illustration for the proposed systems. (a) Stand-alone thermochemical biorefinery, (b) Thermochemical biorefinery including concentrated solar power (CSP) assistance.

2. System description

2.1. Conceptual processes for thermochemical biorefineries

This study models and assesses three concepts of syngas platform biorefineries for biomass-derived DME production. DME is the target product, which is also used to compare the performance of different routes for syngas cleaning and conditioning. Moreover, electricity generation for own consumption or sale (if surplus) is also considered in all concepts. In one of the scenarios, H_2 is included as a high-value co-product. However, the expected yield of these co-products will be determined by the energy integration of each concept, always targeting maximum DME generation. The two main DME synthesis processes are used in the proposed schemes; the direct conversion from syngas in a single reactor (1 step) and the indirect route through the synthesis and dehydration of methanol in two reactors (2 steps) [21]. Nevertheless, depending on the chosen synthesis loop, the syngas must meet the specific requirements of their catalytic reactors. These requirements impact the selection and coupling of the different technological options for the cleaning and conditioning sections of the syngas.

Fig. 1 shows the basic scheme of the process alternatives considered in this study. The process starts with biomass drying and milling operations for subsequent gasification in a dual circulating fluidized bed reactor (DCFBG). Two options were analyzed for the syngas purification section. The first uses an oil scrubber (OLGA) for tar removal, and the second uses a tar cracker/reformer (TR) reactor. These processes are

intended to keep the gas stream free of impurities such as tars, NH_3, H_2S, among others, which can poison catalysts and downstream damage equipment. In addition, clean syngas can be directly used to generate heat and electricity or synthesize several bio-products. However, its conditioning is necessary to meet the specific requirements of each synthesis loop, such as the limit content of light hydrocarbons and CO_2, among others (further details in section 3.1.3).

Three conditioning routes that define the base scenarios were selected (without CSP support). Scenario 1 (SC1), linked to OLGA, is based on a steam reformer (SR), in which the aim is to reduce the light hydrocarbon content. Scenarios 2 (SC2) and 3 (SC3) are linked to the TR option, that in addition to tar cracking, also includes steam reforming. SC2 includes a water gas shift (WGS) unit, and SC3 a pressure swing absorption (PSA) unit. A monoethanolamine (MEA) based absorption system is used for CO_2 recovery in all scenarios. Finally, the direct DME synthesis (1 step) is applied for SC3, and the 2 steps DME synthesis loop is applied for SC1 and SC2.

2.2. Solar integration approach

The concept used to integrate solar energy into the TBRF scenarios is based on a conventional CSP plant for power generation. This scheme will contribute to meeting the plant's electricity needs and exporting the power surplus to the grid. Solar tower (ST) technology was selected due to its maturity and greater suitability for operation with large-capacity TES systems. Fig. 2b shows how the inclusion of the ST plant modifies the operation of the TBRF by redirecting the off-gases (i.e., unreacted syngas from the synthesis loop and distillate lights from the separation train) from the power block to the reforming reactor furnaces (SR or TR depending on the scenario). This modification aims to increase DME production by replacing a fraction of the fresh syngas burned to supply process heat with off-gas. However, this also implies an increase in electricity consumption and a reduction in generation capacity by removing the off-gas fueled combined cycle from the power block (included in the stand-alone scenarios).

In stand-alone scenarios, the high-temperature heat required in endothermic reactors (e.g., DCFBG, SR, TR) is satisfied by burning a portion of the biomass or processing syngas. Similarly, other medium and low-temperature heat needs and process steam are covered by the energy integration of the plant through a heat exchangers network (HEN). In terms of power production, the base scenarios include a combined cycle driven by the off-gas from the synthesis loop. In addition, the amount of residual heat (RESH) available after the plant energy integration will boost the power production (as shown in Fig. 2a). Further details on RESH calculations are provided in section 3.1.4. The plants were designed under the assumption of maximum DME generation. Therefore, no net power generation is expected, and a portion of the electricity will have to be imported from the grid to supply the unmet demand.

Large TES capacities imply significant increases in the operating hours of CSP plants, allowing, for example, an ST plant to reach capacity factors of up to 66% [22]. However, to reach firm supply, such large storage systems are required that are neither technical nor economically feasible [23]. Therefore, in CSP-assisted scenarios, it will still be necessary to import electricity from the grid at certain hours. On the other hand, it is assumed that electricity from RESH maintains the same mode of operation as in the stand-alone scenarios. Thus, CSP variable generation will be added to the stable generation of RESH to supply the entire structure consumption and, when possible, export the surplus. The latter would occur in the hours when the solar resource or the TES allows the CSP block to operate at a capacity greater than the TBRF demand, discounting the RESH generation. Otherwise, consumption coverage will be completed by importing electricity from the grid. Table 1 shows the design basis and summarizes the process options for the six scenarios analyzed in this study: three TBRF stand-alone scenarios and three scenarios, including CSP assistance.

Table 1
Design basis and process concepts for the scenarios assessed in this study.

	SC1	SC2	SC3	SC1-CSP	SC2-CSP	SC3-CSP
Basis of design						
Plant size (MW_{th}, HHV basis)	500	500	500	500	500	500
Energy self-sufficient criterion[a]	✓	✓	✓	✓	✓	✓
Maximum product yield criterion[b]	✓	✓	✓	✓	✓	✓
Power neutral criterion[c]	–	–	–	✓	✓	✓
CSP support	–	–	–	✓	✓	✓
ST plant net capacity (MW_e)	–	–	–	49.5	49.5	49.5
TES capacity (hours)	–	–	–	15	15	15
Expected products						
H_2	–	–	✓	–	–	✓
DME	✓	✓	✓	✓	✓	✓
Electricity for export	–	–	–	✓	✓	✓
Process options						
Oil scrubber (OLGA)	✓	–	–	✓	–	–
Tar cracker/steam reformer	–	✓	✓	–	✓	✓
H_2S removal unit	✓	✓	✓	✓	✓	✓
Steam reformer (SR)	✓	–	–	✓	–	–
Water-gas shift reactor (WGS)	–	✓	–	–	✓	–
CO_2 recovery system	✓	✓	✓	✓	✓	✓
Pressure swing absorption (PSA)	–	–	✓	–	–	✓
Combined cycle power	✓	✓	✓	–	–	–

[a] The only input for process heat generation is biomass.
[b] Unreacted syngas is recirculated as much as possible in the synthesis loop.
[c] Electricity generated in the plant is greater than its consumption on an annualized scale. Notes: **SC1-3:** Scenarios 1 to 3, **CSP:** Concentrated solar power, **DCFBG:** Dual circulant fluidized bed gasifier, **ST:** Solar tower, **TES:** Thermal energy storage.

3. Methodology

3.1. Detailed process modelling

3.1.1. Biomass pretreatment and gasification

A 500 MW_{th} capacity was selected as the design basis, implying a daily consumption of 2140 tonnes of dry biomass. This nominal capacity is widely used in similar studies of biomass-to-liquids (BTL) processes [24,25]. The feed biomass in all scenarios is poplar chips with a high heating value (HHV) of 20.18 MJ/kg on a dry basis. The biomass moisture is reduced from 30% to 12% in a rotary dryer using flue gas from char combustion in the gasifier as an energy source. This gas is pre-cooled in a heat exchanger to 450 °C while generating low-pressure steam (LPS) (2 bar, 140 °C) used in the gasifier. After drying, the biomass undergoes a grinding process to reduce its particle size.

The biomass conversion to syngas is carried out in a dual circulating fluidized bed gasifier (DCFBG) using steam as the gasifying agent. DCFBG was chosen because of its ability to produce syngas with low nitrogen content and because, unlike other gasifiers, it does not require an expensive air separation unit (ASU). The reactor operates at 900 °C and atmospheric pressure (1.5 bar), consuming 0.4 kg of steam per kg of biomass. Besides, the cold gas efficiency is assumed to be 77.07% (HHV basis). DCFBG was modelled according to experimental data from the Battelle Columbus laboratory gasifier [26]. The ultimate analysis of the feedstock biomass and the raw syngas composition is shown in Table 2.

Table 2
Biomass feedstock and syngas composition.

Biomass feedstock Component	% wt., dry basis	Raw Syngas Component	Molar (%)
C	50.9	H_2	14.55
H_2	6.05	CO	23.64
O_2	41.92	CO_2	6.92
N_2	0.17	H_2O	43.43
S	0.04	CH_4	8.43
Ash	0.92	NH_3	0.18
Moisture	30% wt.	TARS	0.15
HHV	20.18 MJ/kg	C_2+	2.7
–	–	H_2S	184 ppm
–	–	Ratio H_2/CO	0.61

3.1.2. *Syngas cleaning and conditioning*

Although the syngas at the gasifier outlet is mainly composed of CO and H_2, it also contains components such as tars, H_2S, NH_3, alkali compounds, among others that must be removed to prevent damage to the downstream process units. In this study, two options for removing tars are considered, tar washing in an oil scrubber (OLGA) or tar cracking and reforming in TR. The use of an oil scrubber is a conservative alternative since it is a reliable technology already tested in pilot and demo plants [27]. TR is an innovative alternative that, despite its moderate technological readiness level (TRL), has been included in several feasibility studies [28–30]. TR is based on a catalytic process that allows adjusting the H_2/CO molar ratio by reforming TAR and light hydrocarbons. However, it requires burning a portion of the syngas that provides additional heat to reach an operating temperature of 930 °C (higher than the gasification temperature). It is assumed that the water content in the syngas is sufficient to run the reaction so that no steam addition is necessary.

The pre-cooled gas passes through a water scrubber to remove NH_3 and HCl in both purification routes. The syngas is then compressed to 20 bar in a 3-stage compression set with intermediate cooling. The compressor's isentropic efficiency is set at 78%, with a maximum compression ratio of 3.5. Sulphur removal (in the form of H_2S) is carried out by LO-CAT® technology, enhanced by a bed filtration unit (i.e., ZnO bed) to ensure a sulphur concentration of less than 0.1 ppm [31,32]. Three process alternatives for gas conditioning are included in this study. These alternatives combine different technological options to meet the downstream requirements according to the synthesis loop of each scenario. Nonetheless, in all cases, the conditioning is based on a unit for adjusting the molar composition of the syngas accompanied by a

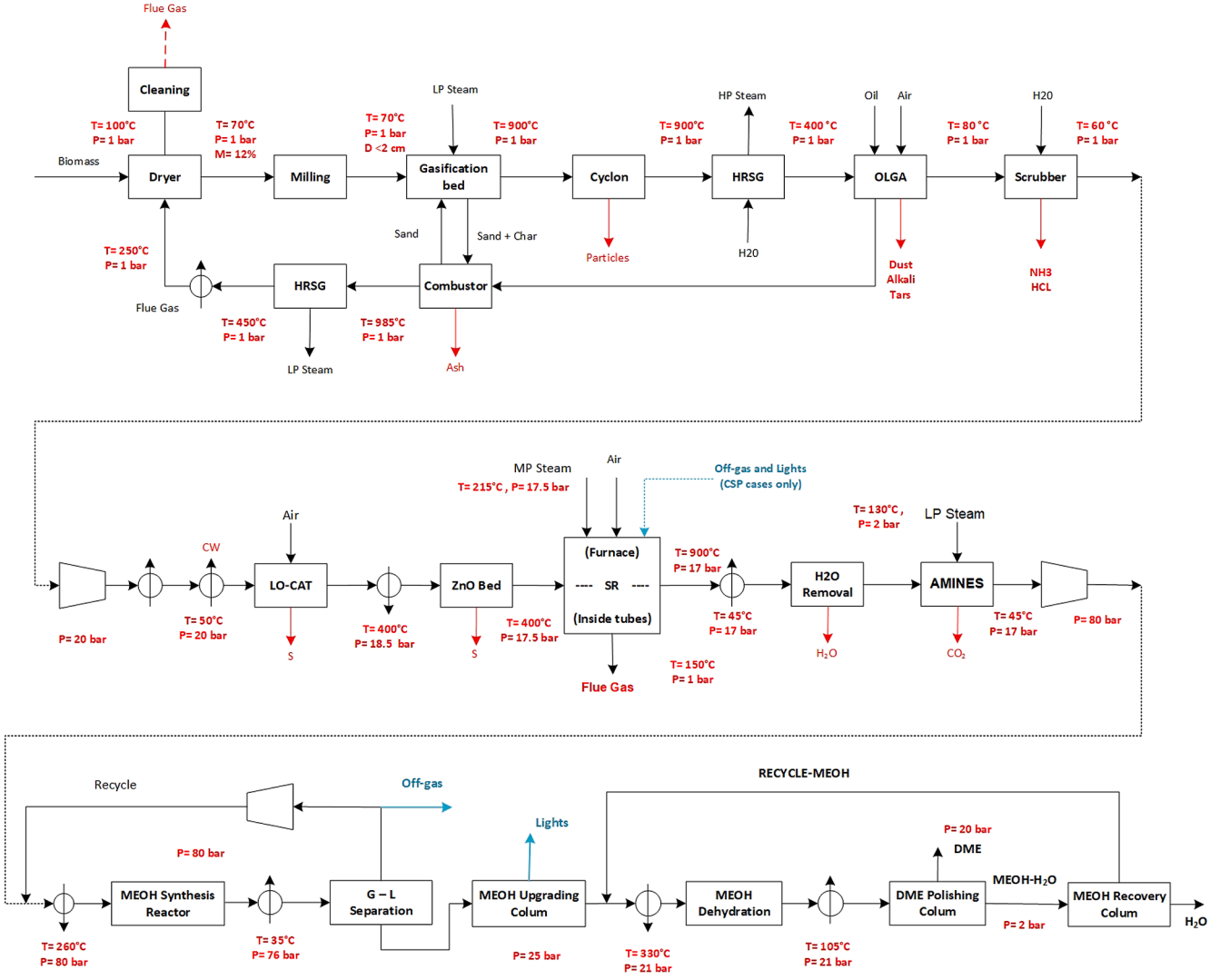

Fig. 3. Flow diagram for SC1 process concept. The dotted blue line includes the variation in the use of off-gas only for the case with CSP assistance (SC1-CSP). (For interpretation of the references to colour in this figure legend, the reader is referred to the web version of this article.)

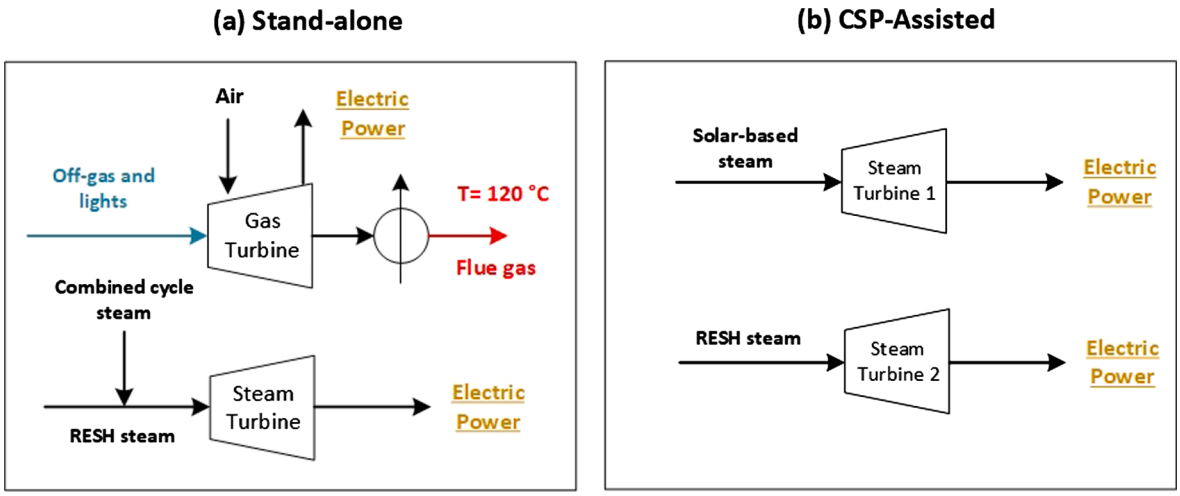

Fig. 4. Power block related to stand-alone (a) and solar-assisted cases (b).

CO_2 removal system.

SR is used in SC1 to convert methane and other light hydrocarbons into syngas. The molar composition is adjusted by varying the steam addition. However, the process requires additional heat input to sustain the operating temperature (900 °C). This extra heat is obtained from burning a portion of the syngas, reducing process efficiency. In SC2 and SC3, the reforming has been previously carried out in the purification section through the TR unit. For SC2, a portion of the desulphurized syngas passes through a WGS reactor to adjust the stoichiometric ratio by generating additional H_2 and converting CO to CO_2 [33]. In SC3, a PSA unit is included to recover H_2 and adjust the H_2/CO molar ratio. The recovered H_2 is compressed to 200 bar for further commercialization as a co-product [34]. CO_2 removal is carried out in all scenarios through a scrubber with a MEA solution [35].

3.1.3. DME synthesis and product separation

The two main routes for DME synthesis were considered in this study. CO and H_2 are converted into DME in a single catalytic reactor for the 1-step route [36]. While in the 2-steps route, methanol is first synthesized and subsequently dehydrated to obtain DME. For the 1-step route, the inlet syngas must maintain an H_2/CO molar ratio in the range of 0.5–2.0 and a molar concentration of light hydrocarbons and CO_2 below 10% and 25%, respectively. For the 2-steps route, the stoichiometric ratio ($S = (H_2\text{-}CO_2)/(CO + CO_2)$) must be equal to 2.0, the hydrocarbon content less than 10% and the CO_2 content can vary in the range of 4–8% (molar basis).

In the 1-step process, the syngas is compressed up to 50 bar and heated up to 230 °C before entering the synthesis reactor. The DME stream leaving the reactor requires cryogenic cooling to achieve a temperature as low as −20 °C to facilitate gas–liquid separation in a degasser. The resulting condensate undergoes a two-step distillation process to separate the hydrocarbons and CO_2 (lights) initially and finally the remaining water. In the 2-step process, the methanol synthesis reactor operates at 80 bar and 260 °C. The stream leaving the reactor passes first through a gas–liquid separator and then through a methanol distillate column. Then, pure methanol is dehydrated to DME in a fixed bed reactor and subsequently sent to a DME distillation column. The unreacted syngas is further compressed and recirculated to increase DME production in both processes. Maximum recirculation is assumed if the requirements at the inlet of the synthesis loop are met, being hydrocarbon concentration the active constraint. Product separation in all scenarios has been adjusted to produce DME with a purity between 99.0% and 99.5%. Further details are given in the supporting information.

3.1.4. Energy integration and power island

Once the TBRF process units are modelled, an exhaustive inventory of all heat sources and heat sinks is performed, including, among other parameters, thermal power and temperature ranges. Based on the information collected, the energy integration of the plant is carried out using the pinch method with a minimum temperature difference (ΔT_{min}) of 20 °C. Then, the grand composite curve is constructed, and the heat exchanger network (HEN) is modelled accordingly. The residual (surplus) heat (RESH) is only quantified when all the thermal needs of the plant have been satisfied. Then, the amount of RESH available at medium and high temperatures (>250 °C) is used to produce high-pressure steam (HPS: 100 bar, 550 °C), which is then expanded in a turbine for power generation. The energy efficiency of this process is assumed to be 37%. According to each scenario, the fixed electricity derived from RESH is either added to the combined cycle generation or the CSP block.

In the stand-alone scenarios, the process off-gas (consisting of unreacted and non-recirculated syngas from the synthesis loop and distillate lights from the separation train) is used for electricity production through a combined cycle unit. Meanwhile, electricity generation comes mainly from the CSP system (including TES) in solar-assisted scenarios. In these cases, the combined cycle is suppressed, and the off-gases are redirected from the power block to the reforming reactors (SR and TR) aiming to reduce the combustion of fresh syngas. The thermal energy supplied by the off-gas to the reforming processes varies in the range of 7.8 to 21.6 MW_{th} depending on the scenario analyzed (this represents between 20 and 46% of the heat duty consumed in the SR or TR units, more details are provided in section 4 of the supporting information). Moreover, available RESH for power generation may vary compared to the stand-alone scenarios due to the increased syngas in the downstream process units (as described in section 4.1). Briefly, CSP-assisted scenarios have a fixed electricity generation from the RESH steam turbine plus a variable generation from the CSP block.

Fig. 3 shows the process flow diagram for scenario SC1 and the variations included for SC1-CSP, while the power block alternatives are shown in Fig. 4. The process diagrams for all scenarios assessed in this study are included in the supporting information. Table A1, included in Appendix A shows the parameters and reactions used to model the main TBRF process units.

3.1.5. Solar tower block and plant location

The CSP block is based on a 50 MW_e (net capacity) ST plant with 15-hour of TES, following the typical size of current operational CSP plants in Spain [37]. In addition, this plant size ensures coverage of TBRFs electricity demand and allows selling surplus (if available) as a co-product. Several technical design parameters are based on the

Table 3
Main parameters used in ST modelling.

Parameter	Value
DNI design point (W/m^2)	850
Solar multiple (-)	2.7[a]
Heliostat reflective area (m^2)	144.4
Total reflective area (m^2)	797 382
TES capacity (hours)	15
Heat transfer fluid (HTF)	Molten salt (60% $NaNO_3$, 40% KNO_3)
HTF cold/hot temperature (°C)	290–565
Tower height (m)	148[b]
Receiver diameter (m)	13.9[b]
Design gross output (MW_e)	55
Net output at design (MW_e)	49.5
Gross to net conversion efficiency (-)	90%
Cycle conversion efficiency (-)	41.20%
Power absorbed in the solar field (MW_{th})	360.4
TES thermal capacity (MW_{th})	2003
Working fluid	Superheated steam
Boiler operating pressure (bar)	100

[a] Optimal value for the selected TES capacity (using the correlation developed by the authors in [22]).
[b] Obtained from solar field optimization algorithm [46].

Gemasolar plant currently operating in the province of Seville (southwest Spain) [38]. Seville was selected as a case study because of its high direct normal irradiance (DNI) (i.e., 5.68 kWh/m^2/day) [39] and due to its location in an area with significant biomass and organic waste resources available for the bioeconomy [40]. From our previous studies, a plant located in Seville would have different biomass sources. However, considering a realistic approach, agricultural wastes would be prioritized to avoid competition with other uses (domestic heating, first-generation biofuels, among others).

Agricultural wastes are highly affected by transportation (low density) and represent a local resource with no current or planned use. In addition, this type of biomass is often found in moderate DNI locations, which is the aim of this study. Considering the selected location of Seville, a plant size of 500 MW_{th} would imply consuming about two-thirds of the available biomass within a radius of 100 km [40]. Therefore, the price used in this study for the reference biomass (66 USD/t) is close to those accepted for agricultural wastes in Spain (approx. 64.5 USD/t) [41]. In addition, considering the need for decentralized collection and in-situ pretreatment of agricultural wastes, their price is not distance-sensitive within the assumed range. Furthermore, a typical meteorological year (TMY) with high-precision ground-based measurements was used as the solar dataset. The data includes measures of DNI, global horizontal irradiance (GHI), ambient temperature, relative humidity and other meteorological variables with hourly resolution [39]. The DNI design point was set at 850 W/m^2, a typical value used for CSP plants operating in Spain [42].

The solar field consists of 5522 heliostats with an area of 144 m^2 each that reflect the irradiation and concentrate it on a single focal point. Heliostats are arranged around a tower that supports a cylindrical receiver in which molten salts circulate, used as HTF and storage fluid. Molten salts are heated in the receiver from 295 °C (cold tank temperature) to 565 °C and sent to the hot tank. Then salts are conducted to the power block or stored according to the generation schedule. The power block is based on a conventional Rankine cycle operating with superheated steam at 100 bar. A gross-to-net efficiency of 90% and a cycle efficiency of 41.2% were set assuming a wet cooling system [43,44]. Parameters such as total reflection area, tower height and receiver diameter are obtained from the SolarPilot optimization algorithm of the *National Renewable Energy Laboratory* (NREL) [45]. In addition, the solar multiple (MS) was set based on the selected TES capacity according to a correlation developed by the authors [22]. Table 3 summarizes the main parameters used in the ST modelling.

3.1.6. Methodological steps and simulation process

The TBRF process alternatives were modelled in detail (as further described in Table A1) using the Aspen Plus® process simulator (version 10). The Redlich-Kwong-Soave with Boston-Mathias alpha function (RKS-BM) thermodynamic model has been applied to the biomass gasification, gas cleaning and conditioning sections and the DME (1-step) and methanol (2-steps) synthesis. In contrast, the Non-Random Two Liquids model with the Redlich-Kwong equation of state (NTRL-RK) was used for modelling the product separation trains and methanol dehydration in the 2-steps DME synthesis [6,24]. Moreover, the hourly electricity generation of the ST plant was simulated using System Advisor Model (SAM) version 2018.11.11, NREL's proprietary software widely used in CSP-related studies [47,48]. The results of Aspen plus and SAM are linked by accounting for the hourly electricity generation of the related systems (please see section 3.1.4).

The methodological steps used to assess the proposed scenarios are described as follows. The performance of the biorefinery is simulated using Aspen plus to obtain the material and energy balances of the process units. An inventory of heat sources and sinks is developed and used to perform the plant's energy integration through the pinch method. Then, the RESH available for power generation is quantified, and the linked power cycle (case-specific) is designed accordingly. In the stand-alone scenarios, the RESH-derived steam is added to the combined cycle of the plant to complete the electricity balance. Whereas, in the solar-assisted scenarios, the RESH generates electricity decoupled from the steam turbine of the CSP block.

The CSP block is simulated through SAM, obtaining the dataset corresponding to the net power output, among other results (e.g., incident and absorbed power in the solar field). Then, the hourly power derived from CSP is added to the RESH electricity to complete the power generation. Dedicated spreadsheets are used to quantify the electricity needs and surpluses of the entire system according to the generation status for each hour. These spreadsheets also include the electricity price dataset from the Iberian day-ahead market (described in section 3.2.2) to calculate the costs and revenues for purchasing and selling electricity (hourly resolution). Finally, technical evaluation parameters are calculated (as described in section 3.3), and the economic study of each scenario is conducted.

3.2. Economic design

The economic analysis is based on the results of the process simulations. The feasibility assessment is carried out using the discounted cash flow analysis (DFCA) methodology. For the CSP-assisted scenarios, parameters such as total plant investment (TPI) and total operation costs (TOC) are obtained from the sum of the values associated with the systems involved (i.e., TBRF and ST blocks). Equations (1) and (2) are used to calculate TPI and TOC, respectively.

$$TPI = DCC_{TBRF} + DCC_{ST} + ICC_{TBRF} + DCC_{ST} \quad (1)$$

$$TOC = FOC_{TBRF} + FOC_{ST} + VOC_{TBRF} + VOC_{ST} \quad (2)$$

3.2.1. Total plant investment

Both direct (DCC) and indirect capital costs (ICC) associated with the biorefinery are calculated from input parameters and ratios used in similar studies. The purchase cost for equipment (PEC) is calculated and scaled according to the mass and energy flows obtained in the simulations for each process unit. The effect of inflation is corrected using the Chemical Engineering Plant Cost Index (CEPCI) and the installation cost by multiplying the PEC of each unit by a specific installation factor (if unknown, it is assumed to be 2.47). Thus, DCC corresponds to the sum of the installation costs of all equipment. Meanwhile, ICC is estimated as a percentage of DCC as carried out in [6]. The reference parameters for calculating the installation costs of the main equipment are shown in Table 4.

Table 4
Input parameters for calculating the DCC of the biorefinery main equipment.

Equipment	Reference costs (MUSD)	Reference year	Base scale	Unit	Scaling factor[a]	Installation factor	Reference
Dryer	0.39	2008	110	dry t/day	0.7	2.47	[6]
Grinding	0.13	2003	2140	dry t/day	1	2.47	[6]
DCFB gasifier	10.7	2010	100	MW_{th} input (HHV)	0.72	2.47	[53]
Filtering (cyclone)	2.7	2008	500	MW_{th} input (HHV)	0.7	2.47	[6]
Oil scrubber (OLGA)	2.3	2008	6131	Nm^3/h (398 °C,1 atm)	0.65	1	Supplier
TR (including combustor)	4.64	2002	34.22	t (input gas)/h	0.65	2.47	[54]
Water scrubber	0.165	1995	23.15	m^3 (input gas)/s	0.7	1[b]	[6]
Gas compressor	5.85	2009	5.44	MW_e	0.7	1.32	[6]
Air compressor	5.44	2009	5.85	MW_e	0.7	1.32	Supplier
LO-CAT system	15.4	2001	27.83	lb (H_2S)/s	0.65	2.47	[6]
ZnO guard bed	0.02	2002	8	m^3 (feed gas)/s	1	3	[6]
SR (including combustor)	41	2002	1277	kmol (output gas)/h	0.6	1	[55]
WGS unit	0.32	2002	98.45	lb/s	0.56	1	[31]
PSA unit	5.46	2002	0.29	kmol (purge)/s	0.74	1.2	[28]
CO_2 recovery system (MEA)	15.4	2001	45.45	t (CO_2)/h	0.65	2.47	[6]
Methanol synthesis reactor	32	2010	30.54	t (MeOH)/h	0.67	1.3	[56]
Methanol dehydration reactor	2.8	2011	2386	kmol (MeOH)/h	0.65	2.47	[29]
DME synthesis section	36.79	2009	2910	mol (feed gas)/s	0.65	2.1	[57]
DME distillation column	0.48	1998	63,478	lb/h	1.32	2.1	[6]
Gas turbine + HRSG	19.09	2003	50	MW_e	0.7	1	[58]
Steam turbine	23.25	2007	50	MW_e	0.7	1	[58]
Heat exchangers[c]	–	–	–	–	–	–	–

[a] Scaling equation: $Cost/Cost_{base} = (Scale/Scale_{base})^n$.
[b] The installation factor is 1 if the base cost already includes the indirect costs.
[c] The purchase cost is calculated as described in [5].

The input parameters for calculating the capital costs associated with ST have been taken from widely accepted practices in CSP systems [49,50]. However, conservative values have been prioritized (i.e., not fully considering the significant cost reductions expected for this technology in the coming years) [51]. Where necessary, the 2018 exchange rate of the European Central Bank is used [52]. Land costs for the entire structure are estimated as 6% of the sum of the DCCs of both blocks. Finally, the summary of the main economic parameters of ST is shown in Table 5. Further details regarding the economic parameters are provided in the supporting information.

3.2.2. Operating costs and other economic assumptions

The fixed operating costs (FOC) of the TBRF are calculated as a percentage of its CCD. The variable operating costs (VOC) are calculated as a function of the system's consumable purchase costs. Expenses and revenues from buying and selling electricity are calculated by multiplying the amount traded by the day-ahead prices set by the Iberian electricity market (MIBEL) for each hour of the year. The 2017 electricity price dataset was obtained from [59,60] and processed and integrated into the economic analysis, as conducted in [61]. It should be noted that the system is assumed to be a price taker due to the priority dispatch in the power system since it is a renewable technology (merit order) [61,62]. The uncertainty on electricity prices variation is included assuming an annual escalation rate of 4%. Table 6 summarizes the parameters used to calculate the operating costs.

The FOC related to the CSP block is calculated as a function of its installed capacity. VOC is calculated as a function of the electricity generated. For FOC, a value of 65 USD/kW-year was set, which is widely accepted and used in economic studies of ST plants [66]. Regarding VOC, 3.5 USD/MWh is common value for CSP plants [66,67]. However, this value does not consider insurance or the complexity added by TES capacity and the integration of the system in a TBRF installation [68]. Therefore, in line with the conservative approach of the study, a value of 5 USD/MWh was set [22]. Furthermore, the internal rate of return (IRR) is calculated by setting the assumed market price for DME in all scenarios and for H_2 in SC3 and SC3-CSP. The DME minimum selling price (DMSP) is calculated as the value that makes the net present value (NPV) zero for a discount rate of 10%. Finally, a capacity factor of 100% has been assumed for TBFR to match its performance with the generation from the CSP block and the hourly electricity prices. The economic assumptions and market prices of the products used for the DFCA are shown in Table 7.

3.3. Analysis of efficiency

In this study, the material and energy flows of the TBRF block have been calculated on an annualized basis, assuming a capacity factor of 100%. This approach includes the effect of variable CSP operation on the electricity balance (generation and consumption). In addition, it also provides a more realistic estimate of energy efficiency and analysis of the effect of solar assistance on the performance of the different scenarios analyzed. Equations 3–5 are used to calculate the overall energy efficiency (η_{th} total), product generation efficiency (η_{th} product) and solar share [3]. Where *CSP Products* and *SA Products* represent the sum of the energy contained in the products of each CSP-assisted scenario and its related stand-alone scenario (e.g., SC1 and SC1-CSP).

The proposed evaluation parameters enable a fair comparison of all the scenarios considering the different kinds of energy quality of the flows involved (biomass feedstock, solar isolation, utilities, and products). The energy contained in the products (i.e., DME and H_2) and the input biomass is calculated based on their HHV (GWh_{th}). Output electricity accounts for the overall amounts exported from the system to the grid. Whereas, to match the electricity imported from the grid with the energy from other system inputs (i.e., feedstock and DNI) a transformation factor from GWh_{th} to GWh_e of 0.35 has been assumed. The DNI collected annually by the solar field is calculated according to equation (6). Where *SF* represents the solar field, the incident power is obtained from the sum of the DNI values of the dataset and the reflection surface by multiplying the area of each heliostat by the total number of heliostats (as described in section 3.1.5).

$$\eta_{th,total} = \sum_{n=1}^{N=8760} \frac{[Products_n(GWh_{th}) + Electricity\,output_n(GWh_e)]}{[Biomass_n(GWh_{th}) + \frac{Electricity\,input_n(GWh_e)}{0.35} + Collected\,DNI_n(GWh_{th})]} \quad (3)$$

$$\eta_{th,product} = \sum_{n=1}^{N=8760} \frac{Products_n(GWh_{th})}{Biomass_n(GWh_{th})} \quad (4)$$

Table 5
Main input parameters for calculating DCC and ICC for CSP block [49,50].

Parameter	Value
Direct capital costs (DCC)	
Solar field (USD/m^2)	140
TES system (USD/kWh_{th})	22
Fixed solar tower cost (MUSD)	3
Receiver reference cost (MUSD)	103
Balance of plant (USD/kW_e)	290
Power cycle (USD/kW_e)	1040
Indirect capital costs (ICC)	
EPC and owner cost	11% of CDC
Contingency	7% of DCC

Notes :

$$Cost_{Tower} = Fixed\ cost_{Tower} \cdot exp[0.0113 \cdot (Tower\ height - \frac{Receiver\ height}{2} - \frac{Heliostar\ height}{2})]$$

$$Cost_{Receiver} = Reference\ cost_{Receiver} \cdot [\frac{Area_{Receiver}}{1571\ (m^2)}]^{0.7}$$

$$Solarshare = \sum_{n=1}^{N=8760} \frac{CSP\ Products_n(GWh_{th}) - SA\ Products_n(GWh_{th})}{Products_n(CSP-assisted)(GWh_{th})} \quad (5)$$

$$Collected\ DNI = \sum_{n=1}^{N=8760} SF\ incident\ power_n(GWh/m^2) \cdot SF\ reflection\ surface(m^2) \quad (6)$$

Table 6
Main input parameters for estimation of operating costs in TBRF.

Fixed operation costs (FOC)	% DCC
Labor	1.56%
Maintenance	1.50%
General expenses	3.07%
Management and operation services	0.44%
Logistics, selling and marketing costs	1.32%
Insurance	0.50%
Total	8.39%
Variable operation costs (VOC)	
Biomass (USD/t dry)	66.00
SR catalyst (USD/kg)[a]	10.30
TR catalyst (USD/kg)[b]	13.29
WGS catalyst (USD/kg)[c]	15.90
Methanol synthesis catalyst (USD/kg)[d]	21.36
Methanol dehydration catalyst (USD/kg)[e]	25.00
DME synthesis (1 step) catalyst (USD/L DME) [6]	0.0044
LO-CAT® chemical (USD/kg sulphur produced) [6]	0.15
MEA chemical and sorbents (USD/t of CO_2) [6]	3.30
Electricity prices annual dataset[f]	–
Electricity price annual scalation rate (assumed)	4.00%
Wastewater (USD/m^3) [6]	0.73
Demineralized water (USD/t) [6]	0.34
Boiler chemicals [63]	0.14% VOC
Gasifier bed material [63]	0.81% VOC
Ash disposal [63]	0.36% VOC

[a] GHSV (standard conditions) = 1780 h-1, 25% catalyst replacement per year [6].
[b] GHSV = 2476 h^{-1}, 0.01% catalyst volume replacement per day [29].
[c] GSHV = 3000 h^{-1} [64].
[d] GHSV = 8000 h^{-1}, 25% catalyst replacement per year [29].
[e] WHSV = 3.8 (Weight Hourly Space Velocity) according to [65], full replacement twice per year.
[f] Dataset of hourly electricity market price in MIBEL [59,60].

Table 7
Other economic assumptions for DFCA.

DFCA economic assumptions	
Debt/equity	0/100%
Plant life	25 years
Depreciation (linear)	10 years
Salvage value	0 M USD
Construction period	1 year
Income tax	30%
Working capital	1-month operating costs
Land[a]	6% DCC
Total operation hours	8760
Product prices	
DME (USD/GJ)[b]	28.18
H_2 (USD/kg)[c]	3.44
Electricity prices annual dataset[d]	–

[a] Including DCC of CSP block for total land costs calculation.
[b] Adapted from the input value used in [69].
[c] Adapted from [70].
[d] Dataset of hourly electricity market price in MIBEL [59,60].

4. Results and discussion

4.1. Technical performance

The inventory of heat sources and sinks was carried out to obtain the grand composite curves (using the pinch method) for each scenario. The results reveal that in all scenarios, the heat released mainly in the DCFBG, TR, and SR combustors is enough to supply the heat and steam demand of the plant and even have some RESH at medium and high temperatures (T > 250 °C). The hourly RESH available for power generation in the stand-alone scenarios was 13, 54 and 87 MW_{th} for SC1, SC2 and SC3, respectively. The use of off-gas as an additional process heat source increased the amount of RESH for SC2-CSP and SC3-CSP to 59 and 91 MW_{th}, respectively. However, it did not affect SC1-CSP, maintaining the same RESH value as SC1. Further details about the plant's energy integration and the grand composite curves are included in the supporting information. These results show a clear impact of the CSP block on the energy integration of the plant, favoring a more efficient use of residual energy sources (off-gas and RESH).

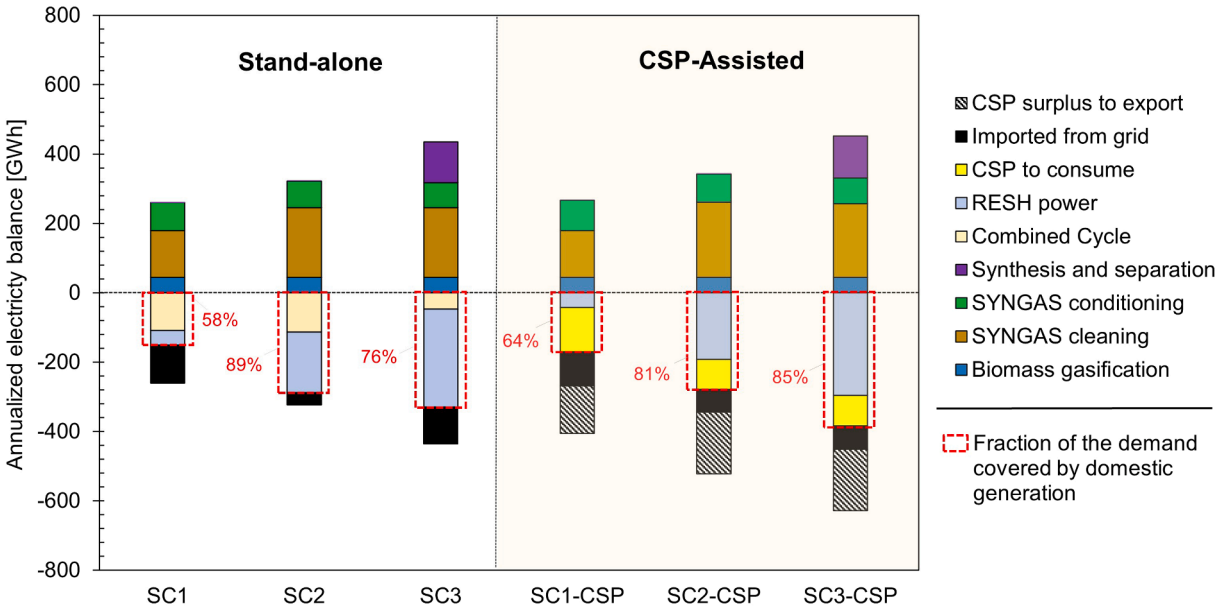

Fig. 5. Annualized electricity balance (including consumption, generation, grid imports and exports).

Fig. 5 shows the balance between generation sources and electricity sinks for all scenarios on an annualized scale. The syngas cleaning section is the main electricity sink, accounting for between 43% and 66% of the consumption in all scenarios, mainly due to syngas and air compression needs. On the one hand, in SC3 and SC3-CSP, the DME synthesis loop (1 step) has a high electricity consumption (up to 27% of the total) due to the cryogenic cooling required for the degassing of the raw DME stream. SC2 has the highest coverage of its electricity demand from its on-site generation (up to 89%). On the other hand, in SC1 and SC3, 42% and 24% of their respective consumptions are covered by imported electricity from the grid. The annual generation from CSP was 265.1 GWh for all scenarios, with a capacity factor of 61.1% and an electrical efficiency of 16%. These values are in line with those reported for operational plants and in other studies for similar solar tower systems [37]. For example, the *Gemasolar* plant located in Seville with 15 h of TES operates with a capacity factor close to 55% [71].

CSP electricity replaces combined cycle generation to cover a portion of domestic consumption in solar-assisted scenarios. However, this generation added to RESH (fixed) electricity is not always available due to the intermittency of solar energy. Although the TES system raises the capacity factor of the ST plant this is not enough to fully supply the demand. Therefore, the electricity balance may vary hourly depending on DNI intensity or TES availability. For instance, importing electricity from the grid at low or zero generation will be necessary to cover consumption. Domestic demand is met, and surpluses are available for export when the CSP system operates at total capacity. SC1-CSP has the highest solar fraction in its electricity consumption with 48% and the highest fraction of electricity imported from the grid, representing 36% of its annual demand. Although SC3-CSP produces the highest amount of electricity (561 GWh/y), SC2-CSP has the highest increase in net

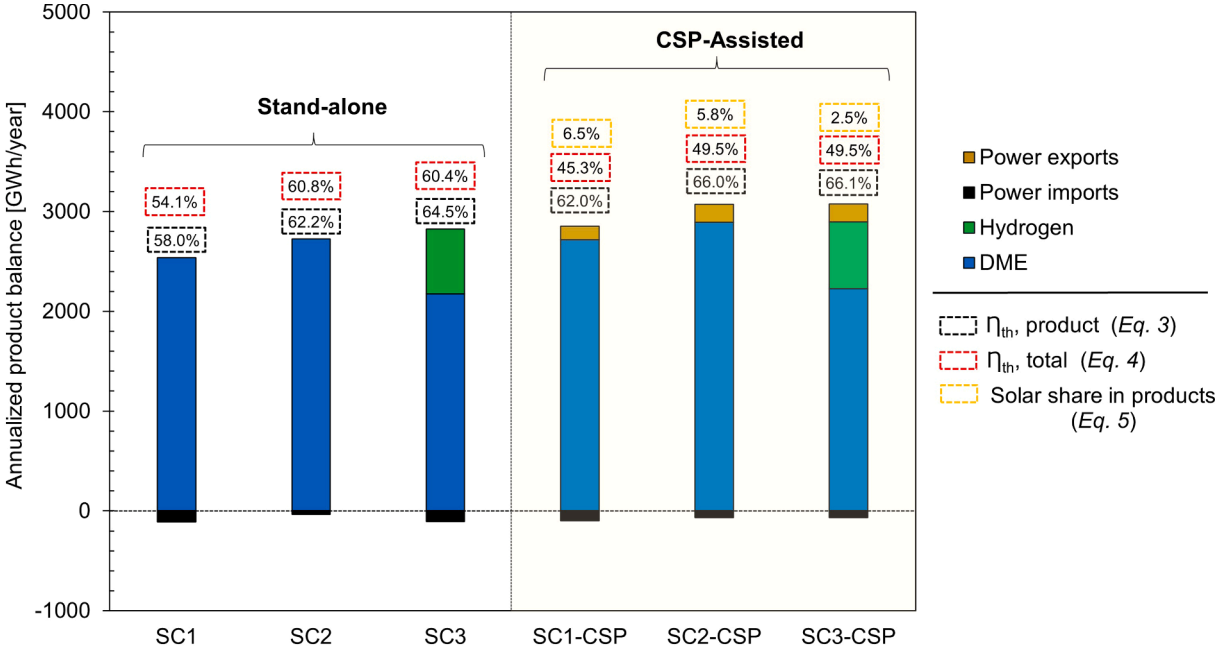

Fig. 6. Energy content of products and main energy conversion efficiencies for each scenario (values given on an annualized basis).

Table 8
Comparison between the stand-alone scenarios in this study and other similar systems in the literature.

	This study	[28]	[72]	[6]	[74]	[75]	[76]	[5]	[24]
Biomass Feedstock	Poplar chips	Switchgrass	Wood pellets	Poplar chips	Poplar chips	Biomass residues	Pulpwood and residues	Poplar chips	Poplar chips
Assessed scenarios	3	2	2	12	5	4	4	6	5
Plant size (MW_{th} on HHV basis)	500	983	>460	500	500	687	604	500	500
Gasifier type	DCFBG	OBFBG	EFG	iCFBG	iCFBG	Pyrolysis	TRIG	EFG	iCFBG
Energy self-sufficient criterion[a]	Yes	Yes	Yes	No	Yes	Yes	Yes	Yes	Yes
Power neutral criterion[b]	No	No	No	No	Yes	Yes	No	Yes	Yes
Target products (other products)	DME (hydrogen and power)	DME and power	DME and power	Polygeneration	EtOH	Naphtha, diesel, and power	FT-jet fuel and power	EtOH	EtOH
Energy efficiency[c]	54.1–60.8%	55–61%	58–64%	34.9–50.2%	31.5–38.2%	62–67.3%	33.7–44.7%	30.2–34.4%	44.3–45.5%
Cold gas efficiency[c]	77.07%	79.80%	81%	77.07%	73–77%	–	–	73.6–74.5%	77.07%
Remarks	Other scenarios include integration with CSP systems	Only DME scenarios were considered	Integrated steam cycle for power generation	DME used as platform chemical	High power consumption limiting global efficiency	Pyrolysis instead of gasification	Only 100% biomass scenarios were considered	High power consumption limiting global efficiency	DME used as platform chemical

[a] The only input for process heat generation is biomass.
[b] No electricity deficit or surplus is expected.
[c] Results range is included for multiple scenarios. Notes: **DCFBG:** Dual circulant fluidized bed gasifier, **OBFBG:** Oxygen-blown fluidized bed gasifier, **iCFBG:** Indirect circulant fluidized bed gasifier, **TRIG:** Transport reactor integrated gasification, **EFG:** Entrained flow gasification; **FT:** Fischer-Tropsch.

generation (112 GWh/y) and the best ratio between electricity exported and imported from the grid (2.7 GWh are exported for every GWh imported).

Fig. 6 shows the total energy and product efficiencies calculated for the six scenarios and the estimated solar share in products for the scenarios with CSP. For the evaluated stand-alone scenarios, the total energy efficiency varied from 54.1% to 60.8%, which is in line with other studies conducted for similar systems. In the study by Larson et al. [28], the evaluated routes for DME and power production achieved energy efficiencies ranging from 54.5% to 61%. Similarly, in the study by Clausen et al. [72], the process schemes evaluated for DME production achieved energy efficiencies between 58% and 64%. These similarities support the validity of the models in this study for predicting the performance of biorefineries based on biomass gasification. An extended comparison, including other similar schemes presented in the literature, is shown in Table 8. The highest total efficiency is achieved in SC2 (60.8%) and SC3 (60.4%), both scenarios with significant electricity generation from RESH. These scenarios use TR as the central unit for syngas cleaning and conditioning. Although SC2 presents a DME production (2724 GWh/y) between 7% and 20% higher than the other base scenarios, the highest product efficiency is achieved in SC3 (64.5%) due to its significant recovery of H_2 (653 GWh/y) as co-product.

Regarding solar-assisted scenarios, SC1-CSP achieves the highest solar share in products (6.5%) due to the higher off-gas power deviated to the reactor burners and the high fraction of solar electricity used to cover its demand. Although CSP assistance contributes to increasing product efficiency by 1.6 (SC3-CSP) to 4 points (SC1-CSP), it also implies a decrease in the total efficiency in the range of 8.8 (SC1-CSP) to 11.3 percentage points (SC2-CSP). That occurs due to the limited solar-to-electricity conversion efficiency of the ST system. The total efficiencies of the CSP scenarios are closer to or even higher than those obtained in similar studies for BTL processes with polygeneration [6]. Furthermore, they can be compared with the maximum energy efficiencies (50%) achieved by other multi-generation systems (i.e., electricity, hydrogen, ammonia, and heating) based on the integration of several conventional renewable technologies [73].

According to the results obtained in this study, the integration of CSP systems to provide utilities to thermochemical biorefineries presents the following advantages: i) the possibility of using the off-gas in higher value applications, e.g., supplying up to 46% of the heat duty required in the reforming processes, ii) dispatchable electricity generation ready to be exported to the grid with the added value of ancillary services and stability, iii) versatile and decoupled designs that could be adapted to the particularities of each site and the technological progress of the available systems, and iv) generating the necessary know-how for the deployment of future solar integration schemes of higher complexity (e.g., solar reactors).

4.2. Investment and operation costs

Fig. 7 shows the breakdown of TPI and TOC for all scenarios analyzed. The TPI is very similar for the stand-alone scenarios, ranging from 481 (SC1, SC3) to 488 (SC2) MUSD. The investment associated with the cleaning section is up to 61% higher for the tar cracking based cases (SC2 and SC3) compared to those using the oil scrubber (SC1). However, the conditioning of SC1 is on average 58% more expensive than SC2 and SC3. On the other hand, the TPIs range from 832 (SC1-CSP) to 841 (SC2-CSP) MUSD for the CSP-assisted scenarios. The significant increase in investment is explained by the high installation costs added by the ST block, which for this study was 6597 USD/kW_e. These results show the effect of CSP on the entire system investment, representing on average 43% of the TPI. However, the impact on operating costs was not as significant, accounting for only 9–10% of the TOC. The purchase of biomass feedstock remains the main operating cost, accounting for around 54% in the stand-alone and 49% in the integrated scenarios.

The purchase of electricity at market price ranged from 2.4 to 7.5 MUSD/y for the base scenarios and from 4.4 to 6.5 MUSD/y for the CSP-assisted scenarios. The Levelized cost of electricity (LCOE) generated in the CSP block was 0.187 USD/kWh. Therefore, purchasing at market price can imply savings of up to 41% of electricity costs compared to assuming the LCOE price. Selling surplus electricity at LCOE price can mean up to 62% additional revenues compared to market prices. Although a priori setting a PPA for the electricity exported to the grid

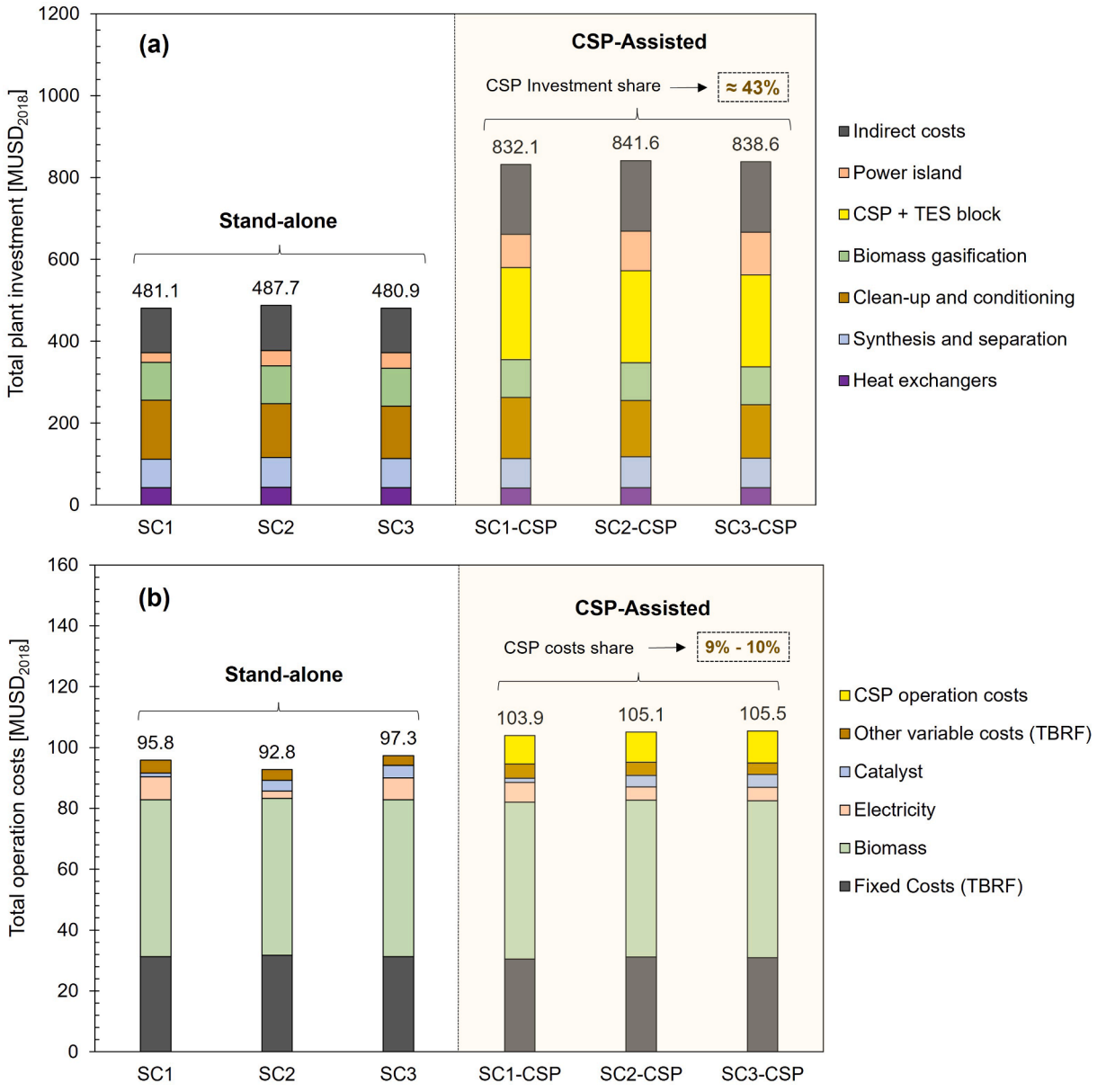

Fig. 7. (a) Total Plant Investment, and (b) Total Operative Costs for each scenario.

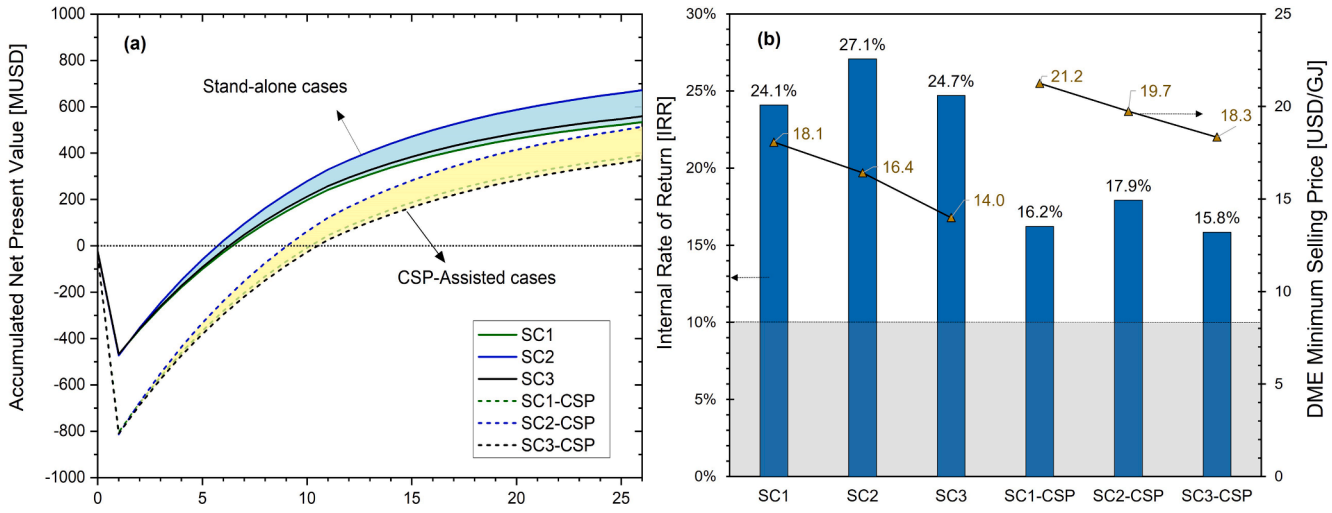

Fig. 8. Main results of the Discounted Cash Flow Analysis (DCFA) for all scenarios. (a) Accumulated NPV, (b) IRR and DMSP.

seems to be the best option, both a substantial increase in the price of electricity and a reduction in the LCOE could reverse this trend. Furthermore, the dispatchable generation of CSP favors purchasing electricity from the grid mainly in the hours with the lowest daily price (i.e., off-peak hours) and selling during hours with the highest prices (peak hours). In summary, the flexibility provided by the CSP would favor a cheap purchase of electricity and an expensive sale.

4.3. DCFA and sensitivity analysis

Fig. 8 shows the cumulative NPV, IRR, and the DMSP for all scenarios analyzed. It can be seen how the NPV of the stand-alone TBRF lies above the area corresponding to the NPV of the CSP-assisted scenarios. In all cases, the NPV is positive, but while the first group becomes profitable around year 6, the second group becomes profitable around year 10. The best economic performance is achieved for SC2 with an IRR of 27.1%. Although the solar-assisted scenarios show a reduction in IRR, they still exceed the benchmark value used in this type of study (IRR = 10%). The sensitivity of IRR to variation in TPI (±40%), product selling price (±40%), electricity price (+100%, −50%) and feed biomass cost (+100%, −50%) was analyzed (Fig. 9). A reduction in the TPI would lead to the most significant economic performance increase in all analyzed scenarios. However, reducing product selling prices (mainly DME) would have the greatest negative effect on process economics. Finally, solar assistance makes the IRR of the biorefineries less sensitive to the variation of all the parameters analyzed.

SC3 achieves the lowest DMSP with 14 USD/GJ, partly because of selling H_2 as a co-product. CSP assistance implies an increase in DMSP in the range of 18% (SC1-CSP) to 31% (SC3-CSP) compared to their base scenarios. However, this impact is limited compared to results reported in similar studies. For instance, a 98% increase in H_2 production cost was reported in [77] for the *"solar-hybrid"* case (molten salt heated membrane reformer) compared to the conventional reference route. One of the scenarios proposed in [8] uses a CSP system as electricity support for converting corn stover to ethanol based on biochemical pathways. A 108% increase in the MSP of ethanol was reported compared to the stand-alone process.

Fig. 10 shows the sensitivity of the IRR to the size variation of the TBRF and CSP blocks. Existing and technologically foreseeable modules were selected as a scaling basis for both systems. For example, three sizes were considered for TBRF (375, 500 and 625 MW_{th} of biomass input), and an additional 50 MW_e block was included for CSP (i.e., overall capacities of 50 and 100 MW_e of power output) for a total of 6 combinations (highlighted in Fig. 10). The highest economic performance is achieved in all scenarios by combining a larger scale TBRF (625 MW_{th}) with a single CSP block (50 MW_e). Similarly, adding a second CSP block (100 MW_e) has a more negative impact on system economics than downscaling the TBRF (375 MW_{th}). The results suggest no apparent scale effect in the evaluated scenarios, as the base cases present similar cost-effectiveness to the cases with the largest scale combination. However, these values may vary depending on the new electricity balances and the fluctuation of other input variables such as electricity and biomass prices. (Further details on the DMSP sensitivity to scale variations are included in the supporting information).

Variations in natural gas prices (the main raw material in the conventional process) highly influence the market price of DME. This influence explains why during the 2021 energy crisis, DME reached a price of up to 28.9 USD/GJ [78], higher than those obtained even in the solar-supported scenarios of this study (DMSP between 18.3 and 21.2 USD/GJ). Prices reported in other studies range from 18.6 USD/GJ for DME derived from natural gas to 50.2 USD/GJ for DME generated from green H_2 (from renewable energy electrolysis) [79,80]. The results presented in this study will provide insights for policymakers in establishing financial mechanisms to promote the construction of integrated renewable polygeneration systems in the near future.

Fig. 11 shows the DMSP sensitivity to the simultaneous biomass cost and electricity prices variation. These parameters present the highest uncertainty within the operating costs. For example, the average monthly balancing price in MIBEL during 2021 fluctuated between 28.5 EUR/MWh in February to 199.9 EUR/MWh in October [81]. Results show that the DMSP is very sensitive to biomass price variation but not much sensitive to changes in electricity prices. However, the impact of the latter parameter is strongly determined by the electricity balance of the system. For instance, in CSP-assisted cases, the negative impact of the increase in biomass cost is partly offset by a positive impact associated with the increase in electricity prices. This is due to the positive electricity balance presented by these scenarios in their exchanges with the grid (i.e., they export more electricity than they import).

The limitations of this study are mainly associated with the particularities of the chosen location. Although the general findings have a broad scope in terms of system performance, other results may be extrapolated only to locations with a comparable DNI (i.e., 5.68 kWh/

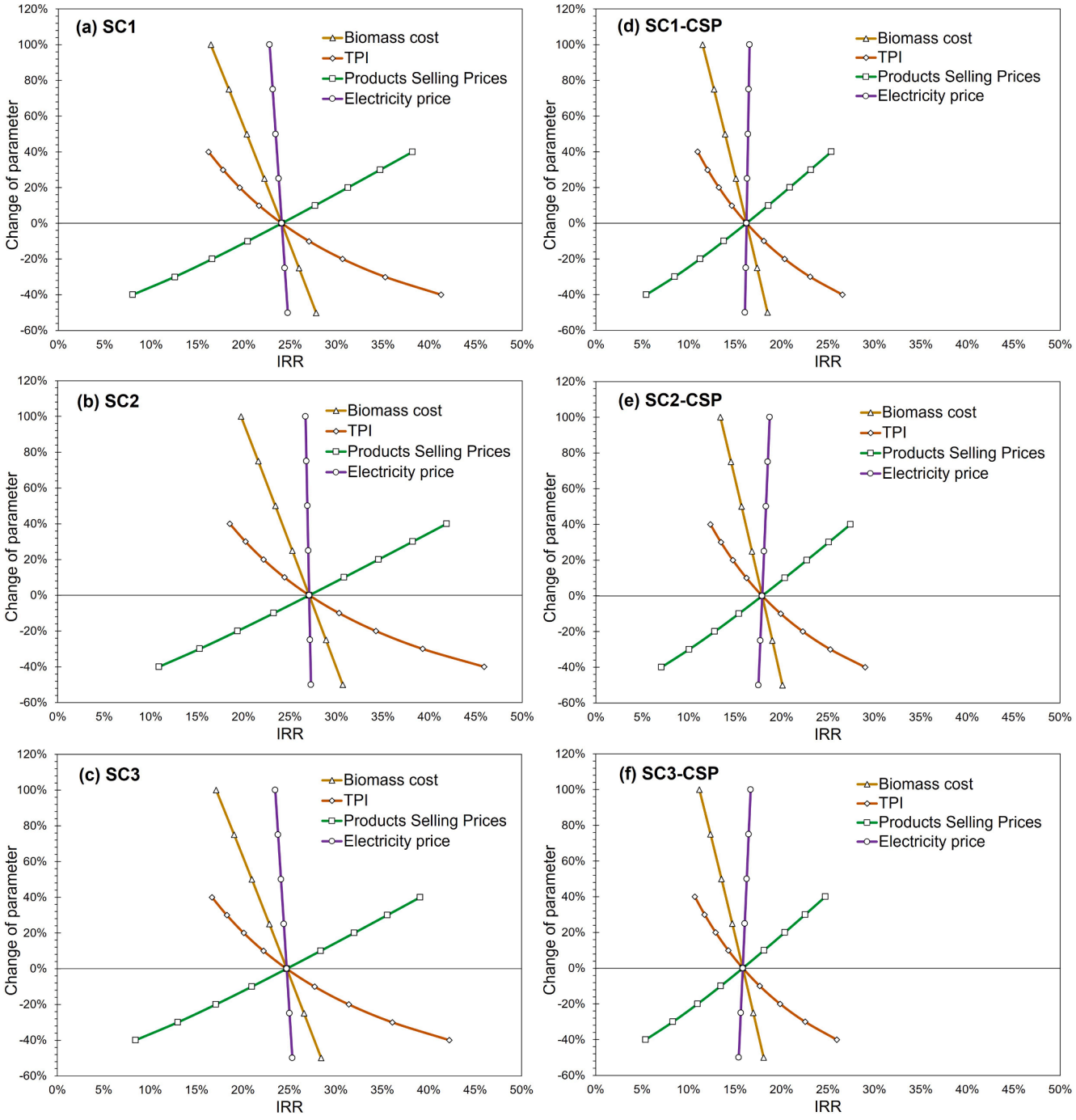

Fig. 9. IRR sensitivity to the variation of the main techno economic variables. (a) SC1, (b) SC2, (c) SC3, (d) SC1-CSP, (e) SC2-CSP, (f) SC3-CSP.

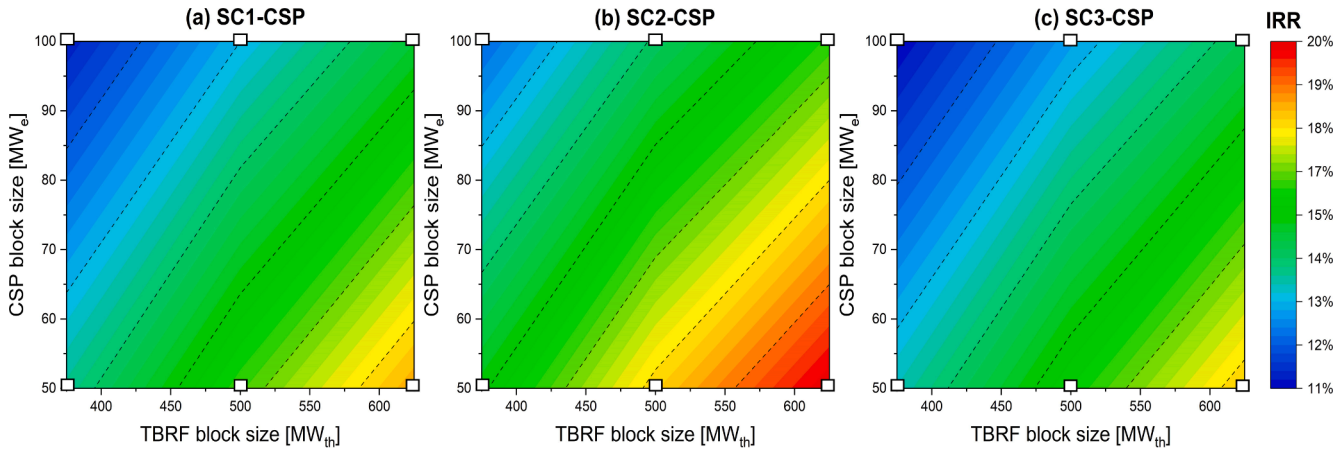

Fig. 10. Internal rate of return (IRR) as a function of various design scales for TBRF (MW_{th} of input biomass) and CSP (MW_e of power output) blocks. (a) SC1-CSP, (b) SC2-CSP, (c) SC3-CSP. The white boxes on the axes represent the size combinations for the cases simulated in this analysis.

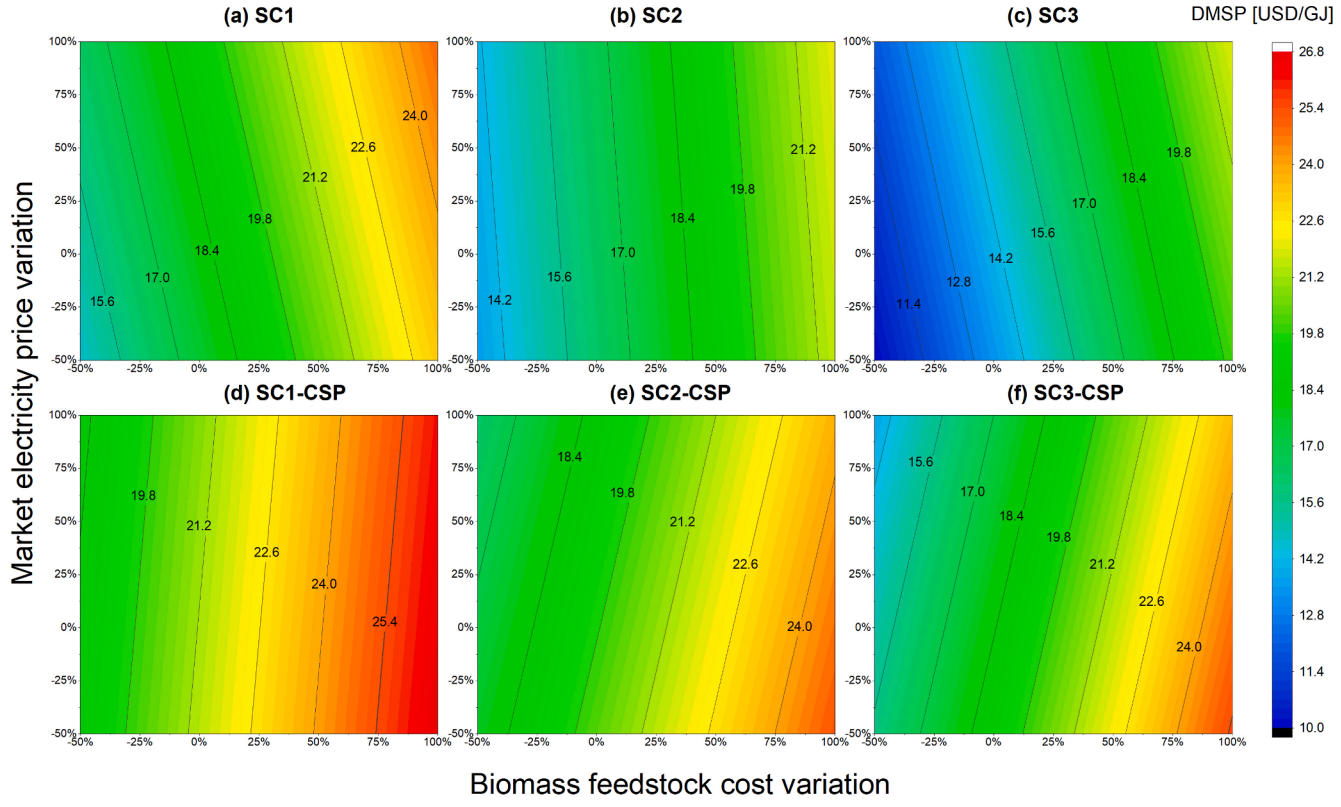

Fig. 11. DME minimum selling price (DMSP) sensitivity to the simultaneous variation of biomass feedstock cost and market electricity price. (a) SC1, (b) SC2, (c) SC3, (d) SC1-CSP, (e) SC2-CSP, (f) SC3-CSP.

m^2/day). Electricity price datasets are also site-specific, which could affect the economic performance of the system when analyzed for markets beyond the Iberian market. Nonetheless, the Iberian market is part of the integrated EU energy market, and therefore, the results of this study are applicable to the whole EU.

It is noteworthy that the economics of all the assessed scenarios may improve if environmental incentives such as emission neutrality credits or even subsidies for CO_2 sequestration are incorporated. In addition, the solar-assisted scenarios could also benefit from other types of subsidies associated with electricity from CSP. Dispatchable renewable energy systems such as CSP are expected to provide stability and ancillary services to power grids; thus, exported electricity could benefit for around 30% tariff increases over the average spot market prices [82]. This study has not considered the potential benefits associated with these mechanisms, which are also under high uncertain because of the future regulatory changes. However, a discussion on these and other financial mechanisms, as well as their role in the deployment of integrated renewable concepts should be addressed in future studies.

5. Conclusions

This study assesses the techno-economic feasibility of thermochemical biorefineries (TBRF) assisted by concentrated solar power systems (CSP). The integration effect on the performance of 3 process alternatives (Table 1) for DME production from gasified biomass (6 scenarios in total) is analyzed. Furthermore, a modular approach was used based on

commercially available solar technologies and focused on electricity generation for self-consumption and sale of surplus to the grid. The main findings are summarized below:

- The stand-alone scenarios presented a negative electricity balance (i.e., they consume more than is generated), covering up to 42% of their demand with electricity imported from the grid. The CSP electricity support changes this trend, favoring positive electricity balances in all scenarios. Although a certain amount of electricity is still imported from the grid (due to the intermittency of solar energy), there is a significant annual surplus of exported electricity.
- In the stand-alone scenarios, the total energy and product efficiencies range from 54% to 61% and 58% to 64%, respectively. Solar assistance moderately increases product energy efficiency (up to 4 points), with a solar share of up to 6.5%. This increase is due to the utilization of off-gases to produce process heat instead of electricity. However, it also reduces the overall efficiency of the plant (up to 11 points) due to the limited electrical efficiency of the CSP block (approx. 16%).
- The inclusion of the CSP block had a significant effect on the investment of the plants but had a minor impact on the operating costs. The internal rate of return (IRR) was reduced by up to 9 points compared to that achieved by the stand-alone biorefineries. Nevertheless, all solar-assisted scenarios achieved an IRR above 10% (reference rate).
- The dispatchability provided by the thermal energy storage system favors the generation of the CSP plants in the hours with the highest daily price in the electricity market. On average, the assisted biorefineries imported electricity from the grid at 0.066 USD/kWh and sold it at 0.069 USD/kWh. This trend could be intensified as the share of variable renewables in the grid increases.
- The sensitivity analysis shows that the impact of uncertainties in TPI and product price amounts to a maximum variation of + 18/-16 points in the base scenarios IRR. Solar assistance reduces the sensitivity to the variation of all parameters. In addition, the effect of the biomass price increase is partly offset by a higher market price for electricity sales.

CSP plants are based on commercially mature technologies that can support the operation of TBRF at an economically viable installed capacity. Although direct integration of solar heat in thermochemical reactors is of great interest to the scientific community, it must first overcome challenges related to the complexity and scalability of the systems involved. The proposed integration of solar energy into thermochemical biorefineries could be a first realistic step towards future polygeneration systems with high synergy between BTL processes and concentrated solar power. The findings of this study are of special relevance for policy makers to promote the integration of CSP systems into "innovative" renewable solutions.

CRediT authorship contribution statement

R.E. Gutiérrez: Conceptualization, Methodology, Data curation, Formal analysis, Software, Writing – original draft. **K. Guerra:** Investigation, Writing – review & editing. **P. Haro:** Conceptualization, Methodology, Validation, Supervision, Writing – review & editing.

Declaration of Competing Interest

The authors declare that they have no known competing financial interests or personal relationships that could have appeared to influence the work reported in this paper.

Data availability

Data will be made available on request.

Acknowledgements

This work was supported by grant PID2020-114725RA-I00 of the project GH2T funded by MCIN/AEI/ 10.13039/501100011033 and by the "European Union". This work was also supported by the Junta de Andalucía through the grant P18-RT-4512 (Co-funded by European Regional Development Fund/European Social Fund "A way to make Europe"). The Ph.D. grant of K. Guerra from Universidad de Sevilla (Spain) under VI PPIT-US is acknowledged. The authors acknowledge A. Gómez-Barea for valuable comments and administrative support during the realization of this work.

Appendix A

See Table A1.

Table A1
Main parameters and reactions used in TBRF modelling.

	Parameter	Value
General equipment		
Pumps	Mechanical efficiency	90%
Compressors	Isentropic efficiency	78%
	Max. pressure ratio	3.5
Process turbines	Isentropic efficiency	72%
Gas turbine	Isentropic efficiency	90%
RESH power cycle	Conversion efficiency	37%
Heat exchangers	Pressure drop	3 psi
Syngas cleaning and conditioning equipment		
Oil scrubber (OLGA)	Tar recovery	99.9%
Water Scrubber	Water/syngas ratio	0.001 m^3
LO-CAT®	Reaction	1) $H_2S + 0.5O_2 \rightarrow H_2O + S$
(Sep and RStoic)*	H_2S recovery	99.9%
	Air/H_2S molar ratio	2.5
Steam reformer	Pressure	17 bar
(RGibbs)*	Temperature	900 °C
	Reactions	Chemical equilibrium (ΔT = 20 °F)
Tar cracker/steam reformer	Pressure	1.4 bar
	Temperature	930 °C
(RStoic and REquil)*	Reactions	1) $CH_4 + H_2O \leftrightarrow CO + 3H_2$ 2) $C_2H_2 + 2H_2O \rightarrow 2CO + 3H_2$ 3) $C_2H_4 + 2H_2O \rightarrow 2CO + 4H_2$ 4) $C_2H_6 + 2H_2O \rightarrow 2CO + 5H_2$ 5) Tar + $2H_2O \rightarrow 10CO + 14H_2$ 6) $2NH_3 \leftrightarrow N_2 + 3H_2$ 7) $CO + H_2O \leftrightarrow CO_2 + H_2$
Gas boiler	Pressure	1.4 bar
(RGibbs)*	Flue gas temperature	150 °C
WGS unit	Reaction	1) $CO + H_2O \leftrightarrow H_2 + CO_2$
(REquil)*	Steam/CO molar ratio	3
MEA bed	Max. CO_2 recovery	90%
	Steam consumption	4.5 MJ per kg of CO_2
PSA unit	Max. H_2 recovery	85%
Synthesis loop equipment		
Methanol synthesis reactor	Temperature	260 °C
	Pressure	80 bar
(REquil)*	Reactions	1) $CO + 2H_2 \leftrightarrow CH_3OH$ 2) $CO + H_2O \leftrightarrow H_2 + CO_2$
Methanol dehydration reactor	Temperature	330 °C
	Pressure	21 bar
(RStoic)*	Reaction	1) $2CH_3OH \leftrightarrow CH_3OCH_3 + H_2O$
DME synthesis reactor	Temperature	280 °C
(REquil)*	Pressure	50 bar
	Reactions	1) $3CO + 3H_2 \leftrightarrow CH_3OCH_3 + CO_2$ 2) $CO + H_2O \leftrightarrow H_2 + CO_2$

* Blocks used for modelling in Aspen Plus. Notes: **WGS:** Water-gas shift, **MEA:** Monoethanolamine, **PSA:** Pressure swing adsorption.

Appendix B. Supplementary data

Supplementary data to this article can be found online at https://doi.org/10.1016/j.apenergy.2022.119535.

References

[1] Creutzig F, Ravindranath NH, Berndes G, Bolwig S, Bright R, Cherubini F, et al. Bioenergy and climate change mitigation: an assessment. GCB Bioenergy 2015;7(5):916–44.

[2] Sorunmu Y, Billen P, Spatari S. A review of thermochemical upgrading of pyrolysis bio-oil: Techno-economic analysis, life cycle assessment, and technology readiness. GCB Bioenergy 2020;12(1):4–18.

[3] Haro P, Arjona R, Ollero P. Thermochemical biorefineries with multiproduction using a platform chemical. Biofuels, Bioprod Biorefining 2014;155–70. https://doi.org/10.1002/bbb.

[4] Brown TR. A techno-economic review of thermochemical cellulosic biofuel pathways. Bioresour Technol 2015;178:166–76. https://doi.org/10.1016/J.BIORTECH.2014.09.053.

[5] Villanueva Perales AL, Reyes Valle C, Ollero P, Gómez-Barea A. Technoeconomic assessment of ethanol production via thermochemical conversion of biomass by entrained flow gasification. Energy 2011;36(7):4097–108. https://doi.org/10.1016/j.energy.2011.04.037.

[6] Haro P, Ollero P, Villanueva Perales AL, Gómez-Barea A. Thermochemical biorefinery based on dimethyl ether as intermediate: Technoeconomic assessment. Appl Energy 2013;102:950–61. https://doi.org/10.1016/j.apenergy.2012.09.051.

[7] Fang Yi, Paul MC, Varjani S, Li X, Park Y-K, You S. Concentrated solar thermochemical gasification of biomass: Principles, applications, and development. Renew Sustain Energy Rev 2021;150:111484. https://doi.org/10.1016/j.rser.2021.111484.

[8] Yakan C, Patel B. Techno - economic study and environmental analysis of a solar - aided lignocellulosic biorefinery : a South African case study. Biomass Convers Biorefinery 2021. https://doi.org/10.1007/s13399-021-01859-2.

[9] Rodat S, Abanades S, Boujjat H, Chuayboon S. On the path toward day and night continuous solar high temperature thermochemical processes: A review. Renew Sustain Energy Rev 2020;132:110061. https://doi.org/10.1016/j.rser.2020.110061.

[10] Bellouard Q, Abanades S, Rodat S, Dupassieux N. Solar thermochemical gasification of wood biomass for syngas production in a high-temperature continuously-fed tubular reactor. Int J Hydrogen Energy 2017;42(19):13486–97.

[11] Li X, Shen Ye, Wei L, He C, Lapkin AA, Lipiński W, et al. Hydrogen production of solar-driven steam gasification of sewage sludge in an indirectly irradiated fluidized-bed reactor. Appl Energy 2020;261:114229. https://doi.org/10.1016/j.apenergy.2019.114229.

[12] Suárez-Almeida M, Gómez-Barea A, Ghoniem AF, Pfeifer C. Solar gasification of biomass in a dual fluidized bed. Chem Eng J 2021;406:126665. https://doi.org/10.1016/j.cej.2020.126665.

[13] Shagdar E, Lougou BG, Shuai Y, Ganbold E, Chinonso OP, Tan H. Process analysis of solar steam reforming of methane for producing low-carbon hydrogen. RSC Adv 2020;10(21):12582–97.

[14] Giaconia A, Iaquaniello G, Caputo G, Morico B, Salladini A, Turchetti L, et al. Experimental validation of a pilot membrane reactor for hydrogen production by solar steam reforming of methane at maximum 550 °C using molten salts as heat transfer fluid. Int J Hydrogen Energy 2020;45:33088–101. https://doi.org/10.1016/j.ijhydene.2020.09.070.

[15] Said SAM, Waseeuddin M, Simakov DSA. A review on solar reforming systems. Renew Sustain Energy Rev 2016;59:149–59. https://doi.org/10.1016/J.RSER.2015.12.072.

[16] Bai Z, Liu Q, Gong L, Lei J. Investigation of a solar-biomass gasification system with the production of methanol and electricity: Thermodynamic, economic and off-design operation. Appl Energy 2019;243:91–101. https://doi.org/10.1016/j.apenergy.2019.03.132.

[17] Wu H, Liu Q, Bai Z, Xie G, Zheng J. Performance investigation of a novel multi-functional system for power, heating and hydrogen with solar energy and biomass. Energy Convers Manag 2019;196:768–78. https://doi.org/10.1016/j.enconman.2019.06.040.

[18] Jie Ling JL, Go ES, Park Y-K, Lee SH. Recent advances of hybrid solar - Biomass thermo-chemical conversion systems. Chemosphere 2022;290:133245. https://doi.org/10.1016/j.chemosphere.2021.133245.

[19] Zanotti M, Ruan Z, Bustamente M, Liu Y, Liao W. A sustainable lignocellulosic biodiesel production integrating solar- and bio-power generation. Green Chem 2016;18(18):5059–68.

[20] DinAli MN, Dincer I. Performance assessment of a new solar energy based cogeneration system for dimethyl-ether and electricity production. Sol Energy 2019;190:337–49. https://doi.org/10.1016/j.solener.2019.08.010.

[21] Azizi Z, Rezaeimanesh M, Tohidian T, Reza M. Dimethyl ether : A review of technologies and production challenges. Chem Eng Process Process Intensif 2014;82:150–72. https://doi.org/10.1016/j.cep.2014.06.007.

[22] Gutiérrez RE, Haro P, Gómez-Barea A. Techno-economic and operational assessment of concentrated solar power plants with a dual supporting system. Appl Energy 2021;302:117600. https://doi.org/10.1016/j.apenergy.2021.117600.

[23] Adinberg R. Simulation analysis of thermal storage for concentrating solar power. Appl Therm Eng 2011;31(16):3588–94. https://doi.org/10.1016/j.applthermaleng.2011.07.025.

[24] Haro P, Ollero P, Villanueva Perales AL, Reyes Valle C. Technoeconomic assessment of lignocellulosic ethanol production via DME (dimethyl ether) hydrocarbonylation. Energy 2012;44(1):891–901. https://doi.org/10.1016/j.energy.2012.05.004.

[25] Haro P, Ollero P, Trippe F. Technoeconomic assessment of potential processes for bio-ethylene production. Fuel Process Technol 2013;114:35–48. https://doi.org/10.1016/j.fuproc.2013.03.024.

[26] Spath PL, Dayton DC. Preliminary Screening – Technical and Economic Assessment of Synthesis Gas to Fuels and Chemicals with Emphasis on the Potential for Biomass-Derived Syngas. Natl Renew Energy Lab 2003:1–160. https://doi.org/10.2172/15006100.

[27] van der Meijden CM, Veringa HJ, Bergman PCA, van der Drift A, Vreugdenhil BJ. Scale-Up of the Milena Biomass Gasification Technology. 17TH BIOMASS Conf Proc 2009.

[28] Larson ED, Jin H, Celik FE. Large-scale gasification-based coproduction of fuels and electricity from switchgrass. Biofuels, Bioprod Biorefining 2009;3:174–94. https://doi.org/10.1002/BBB.137/FORMAT/PDF.

[29] Phillips SD, Tarud JK, Biddy MJ, Dutta A. Gasoline from Wood via Integrated Gasification. Synthesis, and Methanol-to-Gasoline Technologies 2011. https://doi.org/10.2172/1004790.

[30] Susmozas A, Iribarren D, Dufour J. Life-cycle performance of indirect biomass gasification as a green alternative to steam methane reforming for hydrogen production. Int J Hydrogen Energy 2013;38(24):9961–72.

[31] Spath P, Aden A, Eggeman T, Ringer M, Wallace B, Jechura J. Biomass to hydrogen production detailed design and economics utilizing the Battelle Columbus Laboratory indirectly-heated gasifier. 2005.

[32] Iribarren D, Susmozas A, Petrakopoulou F, Dufour J. Environmental and exergetic evaluation of hydrogen production via lignocellulosic biomass gasification. J Clean Prod 2014;69:165–75. https://doi.org/10.1016/J.JCLEPRO.2014.01.068.

[33] Richardson Y, Blin J, Julbe A. A short overview on purification and conditioning of syngas produced by biomass gasification: Catalytic strategies, process intensification and new concepts. Prog Energy Combust Sci 2012;38(6):765–81. https://doi.org/10.1016/j.pecs.2011.12.001.

[34] Makridis SS. Hydrogen storage and compression. In: Carriveau R, Ting DS-K, editors. Methane Hydrog. Energy Storage. London: The Institution of Engineering and Technology; 2016. p. 176.

[35] Kothandaraman A. Carbon Dioxide Capture by Chemical Absorption. A Solvent Comparison Study 2010.

[36] Ohno Y, Yoshida M, Shikada T, Inokoshi O, Ogawa T, Inou N. New Direct Synthesis Technology for DME (Dimethyl Ether) and Its Application. Technology 2006.

[37] Islam T, Huda N, Abdullah AB, Saidur R. A comprehensive review of state-of-the-art concentrating solar power (CSP) technologies : Current status and research trends. Renew Sustain Energy Rev 2018;91:987–1018. https://doi.org/10.1016/j.rser.2018.04.097.

[38] Gemasolar Thermosolar Plant / Solar TRES | Concentrating Solar Power Projects | NREL n.d. https://solarpaces.nrel.gov/project/gemasolar-thermosolar-plant-solar-tres (accessed November 26, 2021).

[39] Moreno-Tejera S, Silva-Pérez MA, Lillo-Bravo I, Ramírez-Santigosa L. Solar resource assessment in Seville, Spain. Statistical characterisation of solar radiation at different time resolutions. Sol Energy 2016;132:430–41. https://doi.org/10.1016/j.solener.2016.03.032.

[40] van der Slikke D, Guerra K, de Jong W, Haro P. The potential of biomass-derived hydrogen in West-Andalusia. In: ETA-Florence Rnewable Energies, editor. Eur. Biomass Conf. Exhib. Proc., Florence: ETA-Florence Rnewable Energies,; 2021, p. 26–9. https://doi.org/10.5071/29thEUBCE2021-5CO.7.1.

[41] Ruiz P, Sgobbi A, Nijs W, Longa FD, Kober T. The JRC-EU-TIMES model. Bioenergy potentials for EU and neighbouring countries. Luxembourg: European Commission 2015. https://doi.org/10.2790/39014.

[42] García GS. Centrales Termosolares CCP Volumen 1: Fundamentos Técnicos. Principales Equipos y Sistemas 2013.

[43] Hirbodi K, Enjavi-Arsanjani M, Yaghoubi M. Techno-economic assessment and environmental impact of concentrating solar power plants in Iran. Renew Sustain Energy Rev 2020;120:109642. https://doi.org/10.1016/j.rser.2019.109642.

[44] NREL. SAM Webinars 2017: Modeling Molten Salt Power Tower Systems in SAM 2017.1.17 2018.

[45] National Renewable Energy Laboratory. System advisor model (SAM). 2019.

[46] SolarPILOT Released as Open Source; Tool Used to Optimize Solar Power Towers | News | NREL n.d. https://www.nrel.gov/news/program/2018/solarpilot-released-open-source.html? (accessed March 31, 2021).

[47] Kost C, Flath CM, Möst D. Concentrating solar power plant investment and operation decisions under different price and support mechanisms. Energy Policy 2013;61:238–48. https://doi.org/10.1016/j.enpol.2013.05.040.

[48] Wagner SJ, Rubin ES. Economic implications of thermal energy storage for concentrated solar thermal power. Renew Energy 2014;61:81–95. https://doi.org/10.1016/j.renene.2012.08.013.

[49] Turchi CS, Heath GA. Molten Salt Power Tower Cost Model for the System Advisor Model (SAM). 2013.

[50] Turchi C. Concentrating Solar Power : Current Cost and Future Directions. Oral Present 2017.

[51] Dieckmann S, Dersch J, Giuliano S, Puppe M, Lüpfert E, Hennecke K, et al. LCOE reduction potential of parabolic trough and solar tower CSP technology until 2025. AIP Conf Proc 2017;160004. https://doi.org/10.1063/1.4984538.

[52] European Central Bank. ECB euro reference exchange rate: US dollar (USD) n.d. https://www.ecb.europa.eu/stats/policy_and_exchange_rates/euro_reference_exchange_rates/html/eurofxref-graph-usd.en.html (accessed May 12, 2020).

[53] Heyne S, Harvey S. Impact of choice of CO2 separation technology on thermo-economic performance of Bio-SNG production processes. Int J Energy Res 2014;38 (3):299–318. https://doi.org/10.1002/er.3038.
[54] Phillips S, Aden A, Jechura J, Dayton D, Eggeman T. Thermochemical Ethanol via Direct Gasification and Mixed Alcohol Synthesis of Lignocellulosic. Biomass 2007.
[55] Simbeck DR, Chang E. Hydrogen Supply: Cost Estimate for Hydrogen Pathways – Scoping Analysis. NREL Tech Rep 2002;NREL/SR-54:71. https://doi.org/NREL/SR-540-32525.
[56] Hannula I, Kurkela E. Liquid transportation fuels bed gasification of lignocellulosic biomass. vol. 91. 2013.
[57] Zhou Li, Hu S, Chen D, Li Y, Zhu B, Jin Y. Study on systems based on coal and natural gas for producing dimethyl ether. Ind Eng Chem Res 2009;48(8):4101–8. https://doi.org/10.1021/ie8006177.
[58] Hamelinck C, Faaij A, Den UH, H b.. Production of FT transportation fuels from biomass; technical options, process analysis and optimization, and development potential. Energy 2004;29:1743–71.
[59] Operador del Mercado Eléctrico (OMIE). OMIE n.d. http://www.omie.es/reports/ (accessed March 14, 2021).
[60] REE. Bienvenido | ESIOS electricidad · datos · transparencia n.d. https://www.esios.ree.es/es?locale=es (accessed March 21, 2021).
[61] Gutiérrez RE, Guerra K, Haro P. Market profitability of CSP-Biomass hybrid power plants: Towards a firm supply of renewable energy. Unpublished manuscript.
[62] Guerra K, Haro P, Gutiérrez RE, Gómez-Barea A. Facing the high share of variable renewable energy in the power system: Flexibility and stability requirements. Appl Energy 2022;310:118561. https://doi.org/10.1016/j.apenergy.2022.118561.
[63] Haro P, Johnsson F, Thunman H. Improved syngas processing for enhanced Bio-SNG production: A techno-economic assessment. Energy 2016;101:380–9. https://doi.org/10.1016/j.energy.2016.02.037.
[64] Torres AIS. Análisis De Sistemas Energéticos Basados En Gasificación De Biomasa 2014.
[65] Hassanpour S, Yaripour F, Taghizadeh M. Performance of modified H-ZSM-5 zeolite for dehydration of methanol to dimethyl ether. Fuel Process Technol 2010; 91(10):1212–21. https://doi.org/10.1016/j.fuproc.2010.03.035.
[66] Kurup P, Turchi CS. Parabolic Trough Collector Cost Update for the System Advisor Model (SAM). 2015.
[67] Malagueta D, Szklo A, Soria R, Dutra R, Schaeffer R, Soares B, et al. Potential and impacts of Concentrated Solar Power (CSP) integration in the Brazilian electric power system. Renew Energy 2014;68:223–35. https://doi.org/10.1016/j.renene.2014.01.050.
[68] International Renewable Energy Agency. RENEWABLE ENERGY TECHNOLOGIES: Cost Analysis of Concentrating Solar Power. vol. 1. 2012. https://doi.org/10.1016/B978-0-12-812959-3.00012-5.
[69] Fornell R, Berntsson T, Åsblad A. Techno-economic analysis of a kraft pulp-mill-based biorefinery producing both ethanol and dimethyl ether. Energy 2013;50: 83–92. https://doi.org/10.1016/j.energy.2012.11.041.
[70] Proost J. State-of-the art CAPEX data for water electrolysers, and their impact on renewable hydrogen price settings. Int J Hydrogen Energy 2019;44(9):4406–13.
[71] SENER. Gemasolar solar thermal power plant n.d. https://www.energy.sener/projects/gemasolar (accessed April 19, 2022).
[72] Clausen LR, Elmegaard B, Houbak N. Technoeconomic analysis of a low CO2 emission dimethyl ether (DME) plant based on gasification of torrefied biomass. Energy 2010;35(12):4831–42. https://doi.org/10.1016/j.energy.2010.09.004.
[73] Wen Du, Aziz M. Flexible operation strategy of an integrated renewable multi-generation system for electricity, hydrogen, ammonia, and heating. Energy Convers Manag 2022;253:115166. https://doi.org/10.1016/j.enconman.2021.115166.
[74] Reyes Valle C, Villanueva Perales AL, Vidal-Barrero F, Gómez-Barea A. Techno-economic assessment of biomass-to-ethanol by indirect fluidized bed gasification: Impact of reforming technologies and comparison with entrained flow gasification. Appl Energy 2013;109:254–66. https://doi.org/10.1016/j.apenergy.2013.04.024.
[75] Meerman JC, Larson ED. Negative-carbon drop-in transport fuels produced via catalytic hydropyrolysis of woody biomass with CO2 capture and storage. Sustain Energy Fuels 2017;1(4):866–81. https://doi.org/10.1039/C7SE00013H.
[76] Kreutz TG, Larson ED, Elsido C, Martelli E, Greig C, Williams RH. Techno-economic prospects for producing Fischer-Tropsch jet fuel and electricity from lignite and woody biomass with CO2 capture for EOR. Appl Energy 2020;279:115841. https://doi.org/10.1016/j.apenergy.2020.115841.
[77] Giaconia A, Iaquaniello G, Morico B, Salladini A, Palo E. Techno-economic assessment of solar steam reforming of methane in a membrane reactor using molten salts as heat transfer fluid. Int J Hydrogen Energy 2021;46(71):35172–88.
[78] China Market Price: Monthly Avg: Organic Chemical Material: Dimethyl Ether: 99.0% or Above | Economic Indicators | CEIC n.d. https://www.ceicdata.com/en/china/china-petroleum–chemical-industry-association-petrochemical-price-organic-chemical-material/cn-market-price-monthly-avg-organic-chemical-material-dimethyl-ether-990-or-above (accessed December 6, 2021).
[79] Lerner A, Brear MJ, Lacey JS, Gordon RL, Webley PA. Life cycle analysis (LCA) of low emission methanol and di-methyl ether (DME) derived from natural gas. Fuel 2018;220:871–8. https://doi.org/10.1016/J.FUEL.2018.02.066.
[80] Tremel A, Wasserscheid P, Baldauf M, Hammer T. Techno-economic analysis for the synthesis of liquid and gaseous fuels based on hydrogen production via electrolysis. Int J Hydrogen Energy 2015;40(35):11457–64. https://doi.org/10.1016/j.ijhydene.2015.01.097.
[81] OMIE. Mínimo, medio y máximo precio de la casación del mercado diario | OMIE n.d. https://www.omie.es/es/market-results/annual/daily-market/daily-prices?scope=annual&year=2021 (accessed December 9, 2021).
[82] Madaeni SH, Sioshansi R, Denholm P. Capacity Value of Concentrating Solar Power Plants 2011.